Engineering Spatial Electron Bridge in Molecular Heterostructure Single-Atom Catalyst for Oxygen Electroreduction

Qiao Gu[1†], Mingtao Huang[1†], Bingyu Huang[2], Wenhui Jiang[1], Ting Hu[1], Dirk Lützenkirchen-Hecht[3], Kai Yuan[1*], Yiwang Chen[1,4*]

[1] College of Chemistry and Chemical Engineering/Film Energy Chemistry for Jiangxi Provincial Key Laboratory (FEC)/Institute of Polymers and Energy Chemistry (IPEC), Nanchang University, Nanchang 330031, China

[2] College of Chemistry and Materials/Key Laboratory of Fluorine and Silicon for Energy Materials and Chemistry of Ministry of Education, Jiangxi Normal University, Nanchang 330022, China

[3] Faculty of Mathematics and Natural Sciences-Physics Department, Bergische Universität Wuppertal, D-42119 Wuppertal, Germany

[4] College of Chemistry and Chemical Engineering, Gannan Normal University, Ganzhou 341000, China

*Corresponding Author(s): kai.yuan@ncu.edu.cn (K. Yuan); ywchen@ncu.edu.cn (Y. Chen)

†Q. Gu and M. Huang contributed equally to this work.

EXPERIMENTAL SECTION

Materials.

2,9-Dichloro-1,10-phenanthroline (97%, Energy Chemical), Iron(III) nitrate nonahydrate ($Fe(NO_3)_3$, 98%, J&K Scientific), 4-Aminopyridine (98%, Macklin), 4-Aminophenol (96%, Energy Chemical), 4-Aminothiophenol (99%, Macklin), multi-walled carbon nanotubes (CNT, OD:10-20 nm, length: 10-30 nm, >95%, XF NANO), tert-butyl nitrite (90%,Energy Chemical), N,N-dimethylformamide (DMF, AR, XiLong science), acetonitrile (AR, XiLong science), tetrahydrofuran (THF, AR, XiLong science), acetone (AR, XiLong science), potassium hydroxide (KOH, 95%, Energy Chemical), zinc acetate ($Zn(OAc)_2$, 99.5%, Energy Chemical). Except for multi-walled carbon nanotubes, other chemicals used in the synthesis of electrocatalysts were obtained from commercial sources and were used without further purification. Deionized water (DIW) was obtained from Direct-Q 5UV system.

Synthesis of $phen_2N_2$.

The synthesis of $phen_2N_2$ was carried out via chemical vapor deposition (CVD) using 2,9-dichloro-1,10-phenanthroline (100 mg) as the precursor. The reaction was conducted under a continuous ammonia flow (10 mL min^{-1}) at 300 ℃ for 11 h. After cooling to room temperature, the product was collected from the crucible, washed with methanol and filtered. Finally, the product was vacuum dried at 60 ℃ for 24 h to obtain $phen_2N_2$.

Synthesis of $Fe(Phen)_2$.

0.1 mmol of $phen_2N_2$ and 6 ml of DMF were put into a round-bottomed flask and sonicated for 30 min, followed by three times of pumping and gas exchange during stirring to a nitrogen environment. Subsequently, 0.3 mmol $Fe(NO_3)_3{\cdot}9H_2O$ dissolved in 2 mL DMF was added under a nitrogen environment. The flask was sealed, heated to 145 ℃, and stirred vigorously for 24 h. After cooling to room temperature, the mixture was filtered and washed with DMF three times, and then vacuum dried at 60 ℃ for 24 h to obtain $Fe(Phen)_2$.

Purification of CNT.

The pristine CNT was purified by heating in air at 400 ℃, followed by acid washing (6

M HCl, 80 ℃, 12 h). After neutralization via water washing and vacuum drying, it was annealed at 900 ℃ under nitrogen to remove residual oxygen groups and adsorbed species.

Synthesis of functionalized CNT (CNT-X).

Initially, 50 mg of purified CNT and 2.5 mmol 4-aminophenol were separately dispersed in 50 mL anhydrous acetonitrile under ultrasonic treatment for 30 min. The 4-aminophenol solution was subsequently introduced into the CNT dispersion and stirred for 10 min. Following this, 15 mmol tert-butyl nitrite was introduced into the reaction system and maintained at 40 ℃ for 24 h. After cooling to room temperature, the dispersion was filtered and washed with acetonitrile, acetone, tetrahydrofuran, and ethanol to obtain CNT-O. CNT-N and CNT-S were prepared in the same procedure as CNT-O, except that 4-aminophenol was replaced by 4-aminopyridine and 4-aminothiophenol, respectively.

Synthesis of CNT-Fe and CNT-X-Fe.

The purified CNT and $Fe(Phen)_2$ were independently dissolved in dimethylformamide (DMF) and sonicated for 30 min. Then the $Fe(Phen)_2$ solution was gradually added to the purified CNT suspension through dropwise addition, followed by continuous stirring at 95 ℃ for 24 h. After natural cooling to room temperature, the product was filtered and washed with DMF, acetone, ethanol, and deionized water. The CNT-Fe was ultimately obtained after vacuum drying at 60 ℃ for 24 h. CNT-X-Fe was synthesized under identical conditions to CNT-Fe, with purified CNT substituted by CNT-O, CNT-S, and CNT-N.

Experimental Procedures

Characterizations

SEM measurements were performed via a scanning electron microscope (JEOL JSM-7900F). TEM images, HRTEM images, SAED patterns, EDS and HAADF-STEM were performed by a scanning transmission electron microscope (JEOL, JEM-2100F). The AC HAADF-STM measurement was performed by a scanning transmission electron microscope (Titan Cubed Themis G2 300). FT-IR spectra were recorded on a

SHIMADZU IRPrestige21 spectrometer. XRD patterns were obtained by a Bruker D8 Advance X-ray diffractometer. Raman spectroscopy was performed on a HORIBA Scientific LabRAM HR Raman spectrometer system. XPS spectra were recorded on a Kratos AXIS Ultra. Ultraviolet-Visible (UV-Vis) absorption spectra were recorded on an Agilent series UV-Vis-NIR spectrophotometer.

XAFS measurements

The Fe K-edge X-ray absorption spectra measurements were conducted at beamline BL10 at the DELTA storage ring (Dortmund, Germany) operating with 100-130 mA of stored 1.5 GeV electrons equipped with a Si (111) double crystal monochromator for energy selection. For these experiments, the X-rays from the wiggler source were monochromatized by a Si (111) channel-cut monochromator, and N_2-filled ionization chambers were employed as detectors for the incident and transmitted X-ray intensities. The samples were homogeneously distributed on a sample holder with a loading sufficient for high-quality XAFS data.

Electrochemical measurements

Electrochemical characterization was performed on AutoLab PGSTAT302Nl with PINE AFMSRCE. All electrochemical measurements are tested using a three-electrode cell system. A rotating disk electrode (RDE) with a geometrical surface area of disk (0.1963 cm^2) or rotating ring-disk electrode (RRDE) with a geometrical surface area of disk (0.2475 cm^2) and ring (0.1866 cm^2) (Pine Research Instrumentation, USA) coated with the electrocatalysts was served as the working electrode. A graphite rod and an Ag/AgCl electrode (3M KCl) were used as the counter electrode and reference electrode, respectively. The electrolyte was O_2 purged 0.1 M KOH aqueous solution.

Preparation of the Working Electrode

At first, 3 mg catalyst was mixed with 245 µL of isopropyl alcohol, 40 µL water and 15 µL of 5 wt% Nafion solution and sonicated for 60 min to obtain a homogeneous ink.

Next, 10 μL of the catalyst dispersion was pipetted onto a glassy carbon surface with a diameter of 5 mm and dried at room temperature.

CV and RDE Measurements

The RDE experiments were conducted at a scan rate of 10 mV/s between -0.95-0.05 V vs. Ag/AgCl under different rotating speeds. Before the measurements, O_2 was purged into the cell for 30 min and maintained during the experiments to ensure O_2 saturation in 0.1 M KOH electrolyte. The potential measured in this study was aligned to the reversible hydrogen electrode (RHE) scale by using the Nernst equation from Ag/AgCl.

$$E_{RHE} = E_{Ag/AgCl} + 0.059pH + E^{\theta}_{Ag/AgCl}\ ^{1} \quad (1)$$

where $E_{Ag/AgCl}$ was the measured potential using Ag/AgCl, and $E^{\theta}_{Ag/AgCl}$ is the standard potential of Ag/AgCl (0.1976 V).

The number of electrons transferred (n) and kinetic current density (j_k) for ORR can be determined from the Koutecky-Levich equation:

$$\frac{1}{j} = \frac{1}{j_L} + \frac{1}{j_k} = \frac{1}{B\sqrt{\omega}} + \frac{1}{j_k} \quad (2)$$

$$B = 0.62nFC_0(D_0)^{2/3}v^{-1/6} \quad (3)$$

$$j_k = nFkC_0 \quad (4)$$

where j, j_k and j_L are the experimentally measured, kinetic and diffusion limiting current densities, respectively, ω is the angular velocity of the rotating electrode ($\omega = 2\pi N$, N is the linear rotation speed), n is the electron transfer number, k is the electron transfer rate constant, F is the Faraday constant (F = 96485 C mol^{-1}), D_0 is the diffusion coefficient of O_2 in 0.1 M KOH (1.9×10^{-5} cm^2 s^{-1}), C_0 is the bulk concentration of O_2 in the electrolyte (1.2×10^{-3} M), and v is the kinematic viscosity (0.01 cm^2 s^{-1}).

The electrochemically active surface area (ECSA) was determined by measuring the capacitive current associated with double-layer charging from the scan-rate dependence of the CV. This measurement was performed on the same working electrode in a potential window of 1.0 - 1.1 V vs. RHE and scan rates ranging from 1.0 to 10.0 mV s^{-1}. Then linear fitting of the charging current density differences ($\Delta_j = j_a - j_c$ at a potential of 1.05 V vs RHE) against the scan rate was done. The slope is twice the

double-layer capacitance C_{dl}. ECSA was calculated using ECSA = $R_f/m_{loading}$, where $m_{loading}$ is the loading mass of catalyst per geometrical area of the electrode. $R_f = C_{dl}/40$ μF cm^{-2} (the average specific capacitance of a flat standard electrode with 1 cm^2 of real surface area is 40 μF cm^{-2}).

RRDE Measurements

Preparation of working electrodes involved the same procedure as described above. The ORR occurs on the disk electrode, while the intermediate product will be thrown to the ring electrode. The yield of HO_2^- (%) and the *n* were calculated by the following equations:

$$n = \frac{4 I_{Disk}}{I_{Disk} + \frac{I_{Ring}}{N}} \quad (5)$$

$$\%(HO_2^-) = \frac{200 \times I_{Ring}}{I_{Disk} + I_{Ring}/N} \quad (6)$$

where I_{Disk} and I_{Ring} are the disk and ring currents, respectively. *N* is the ring current collection efficiency, which is determined to be 0.37.

Scanning electrochemical microscope (SECM)

The SECM measurements were performed on a CHI920D, including a bipotentiostat and a high-resolution 3D electrode positioner. The probe was a CHI116 10 μm Pt SECM tip. The substrate was a home-made concave Au electrode with a recessed microdisk with a diameter of 25 μm at the depth of ~7 μm. An Ag/AgCl electrode was used as reference electrode. A Pt wire was used as counter electrode. The electrolyte was Ar-saturated 0.1 M KOH aqueous solution with 0.5 mM FcMeOH.[2]

To load the catalysts into the concave electrode, catalyst powder was spread onto the surface of glass slide. Then, the concave electrode was gently pressed onto the catalyst powder along the vertical direction, and any residuals were removed with a lens wiping paper. An optical microscope was used to check the loading and flatness. The procedure was repeated several times, until the cavity was filled with catalyst powder.

The probe approach curve technique was used to position z-axis and adjust the platform. The probe was biased at 0.5 $V_{Ag/AgCl}$ to oxide FcMeOH to $FcMeOH^+$. When the probe approaches very close to the surface of the substrate, the feedback current will be greatly changed due to the restricted diffusion. A cut off set at a current level of 75% to avoid crash. A quiet time set for 20 s to steady current value. The adjustment of the platform was based on the three-point fix method.

The SECM technique was used to locate the catalyst region. The probe was biased at 0.85 $V_{Ag/AgCl}$ and the substrate was biased at -0.9646 $V_{Ag/AgCl}$. Firstly, a 500 × 500 μm scan (5 μm/step) was performed for rough locating. Subsequently, a 200 × 200 μm scan (2 μm/step) was performed for fine positioning. The probe returned back to origin when the measurement finished. A quiet time set for 20 s to steady current value. The SECM images were recorded in this 200 × 200 μm region, but changing a series of the given substrate bias potential ranged from -0.9646 $V_{Ag/AgCl}$ to -0.0646 $V_{Ag/AgCl}$.

Surface-interrogation SECM (SI-SECM) measurement

The SI-SECM was performed on the same platform as SECM, including the instrument, electrodes and electrolyte. Firstly, the C_{dl} was measured by a series of CV scanning in a non-Faradaic potential (0.05 - 0.15 V vs. RHE) at given scan rates of 10, 20, 30, 40 and 50 mV s^{-1}. The $ECSA_{UME}$ (subscript UME is to declare the data obtained from ultra-micro electrode) was determined by the same procedure as described in the previous electrochemical measurements section. Subsequently, the Pt tip was electrochemically cleaned by CV cycling from -0.9646 $V_{Ag/AgCl}$ to -0.4646 $V_{Ag/AgCl}$ at 50 mV s^{-1} for ~300 s. Then, the probe was switched to open circuit and the substrate was subject to a given bias potential from -0.9646 $V_{Ag/AgCl}$ to 0.2354 $V_{Ag/AgCl}$ for 30 s. After that, the substrate was immediately switched to open circuit while the probe was biased at 0.4 $V_{Ag/AgCl}$ for 30 s. The feedback current at the probe (I_{tip}) was recorded. The electric quantity at tip (Q_{tip}) was derived by background subtraction and integration of I_{tip}. The active site density (SD) was followed by the relation as described by the following equation:

$$SD = \frac{Q_{tip}/F \times N_A}{ECSA_{UME}} \quad (7)$$

where F represents the Faraday's constant (96485 C mol^{-1}) and N_A is the Avogadro constant (6.02×10^{23} mol^{-1}).

The turnover frequency (TOF) was calculated by following equation:

$$TOF = \frac{N_A \times j_m}{SD_{mass} \times F} \quad (8)$$

The kinetic mass activity (j_m) for the as-papered catalysts in this work is defined as:

$$j_m = \frac{j_k}{m_{catalyst}} \quad (9)$$

where $m_{catalyst}$ is the catalyst loading on the glassy carbon disc (mg cm^{-2}), the potential to determine kinetic current density (j_k) is chosen at 0.8 V.

Variable-Frequency Square Wave Voltammetry (SWV) measurements.

Variable-frequency square wave voltammetry tests were performed in N_2-saturated 0.1 M KOH electrolyte with a step potential of 10 mV and amplitude of 25 mV. The perturbation frequency (f) was varied from 1250 to 0.33 Hz.

Electron transfer reaction between catalysts and TCNQ

5 mg of catalyst was exposed to 5 mL 7.65 mM TCNQ acetonitrile solution in centrifuge tube through ultrasonic treatment, followed by stirring the suspension at 70 °C for 20 min to accelerate the electron transfer reaction. Subsequently, the supernatant is separated by centrifugation for further analysis by UV-Vis absorption spectra. The original TCNQ solution was diluted 250-fold with acetonitrile before measurement. The TCNQ solution that reacted with the catalyst was diluted 2-fold with acetonitrile before measurement.

Calculate k_s by Laviron equation

The $[Fe(CN)_6]^{3-}$ redox process of CNT-Fe and CNT-X-Fe coated glassy carbon electrode and Au electrode at different scan rates (0.005-0.23 V/s) were carried out in 0.1 M KCl. The k_s was calculated with the Laviron equation:

$$E_{p,a} = E^{0'} + \frac{RT\ln \upsilon}{(1 - \alpha)nF} \quad (10)$$

$$E_{p,c} = E^{0'} + \frac{RT\ln \upsilon}{(1 - \alpha)nF} \quad (11)$$

$$\log k_s = \alpha\log(1 - \alpha) + (1 - \alpha)\log\alpha - \log(\frac{RT}{nF\upsilon}) - \frac{\alpha(1 - \alpha)nF\Delta E_p}{2.3RT} \quad (12)$$

Herein, $E_{p,a}$ is the potential of oxidation peak and $E_{p,c}$ is the potential of reduction peak. R is the universal gas constant, F is the Faraday constant, T is the Kelvin temperature, n is the number of electrons transferred, α is the transfer efficiency, ν is the scan rate, and ΔE_p is the potential difference of redox peak.

Liquid Zn-Air Battery Assembly.

A homemade liquid Zn-air battery was fabricated for the evaluation of battery performance. It was constructed by pairing CNT-X-Fe and Pt/C loaded onto a carbon paper with a Zn plate (0.20 mm thickness) in 6 M KOH. The batteries were organized via the following procedure: First, the air electrodes were prepared by pipetting catalyst slurry carefully onto the carbon paper (1.25 mg cm^{-2}) with the help of pipette. Subsequently, polished zinc plates were served as the anode. Battery tests were carried out at room temperature under ambient atmosphere with a CHI 760E and a LAND CT2001A. The specific capacity and energy density can be obtained from the consumed Zn (gently polished and ultrasonically washed several times to remove byproducts or Zn dendrites) after discharge.

Membrane electrode assembly (MEA) preparation and fuel cell tests

A MEA test was applied to measure a single fuel cell performance on fuel cell test station (Scribner, Inc., 850), where CNT-O-Fe was used as the cathode catalysts. The catalyst ink was prepared by ultrasonically mixing the catalyst, 5 wt% Nafion solution

and isopropanol for 1 hour, and followed by the ink was coated on the one side of the Grade 60 membrane (Sustainion, USA) to form the cathode catalyst layer. A commercial PtRu/C (60 wt%) catalyst was prepared by the similar method and sprayed on the other side of the membrane as the anode. The CNT-O-Fe loading was 2 mg cm^{-2} at the cathode and Pt loading was 0.10 mg cm^{-2} at the anode. Subsequently, the SGL-29BC carbon paper was directly applied as the gas diffusion layer (GDL). The SGL-29BC carbon paper was hot-pressed onto the both sides of a Grade 60 membrane (Sustainion, USA) at 120 ℃ for 2 min under a pressure of 2 MPa to make the final MEA with an active area of 5 cm^2, and assembled into a single fuel cell with single-serpentine flow channels. Pure H_2 and compressed air were employed to the anode and cathode for a H_2/air single fuel cell test. During the MEA test, the gas humidification and cell operating temperature were maintained at 80°C, the relative humidity reached 100%, and the back pressure of both the anode and cathode was 0.2 MPa. The cells were activated at 0.3 V, 100% relative humidity and 80 °C, and until the steady state current was reached. Then, fuel cell polarization curves were recorded in a current control mode.

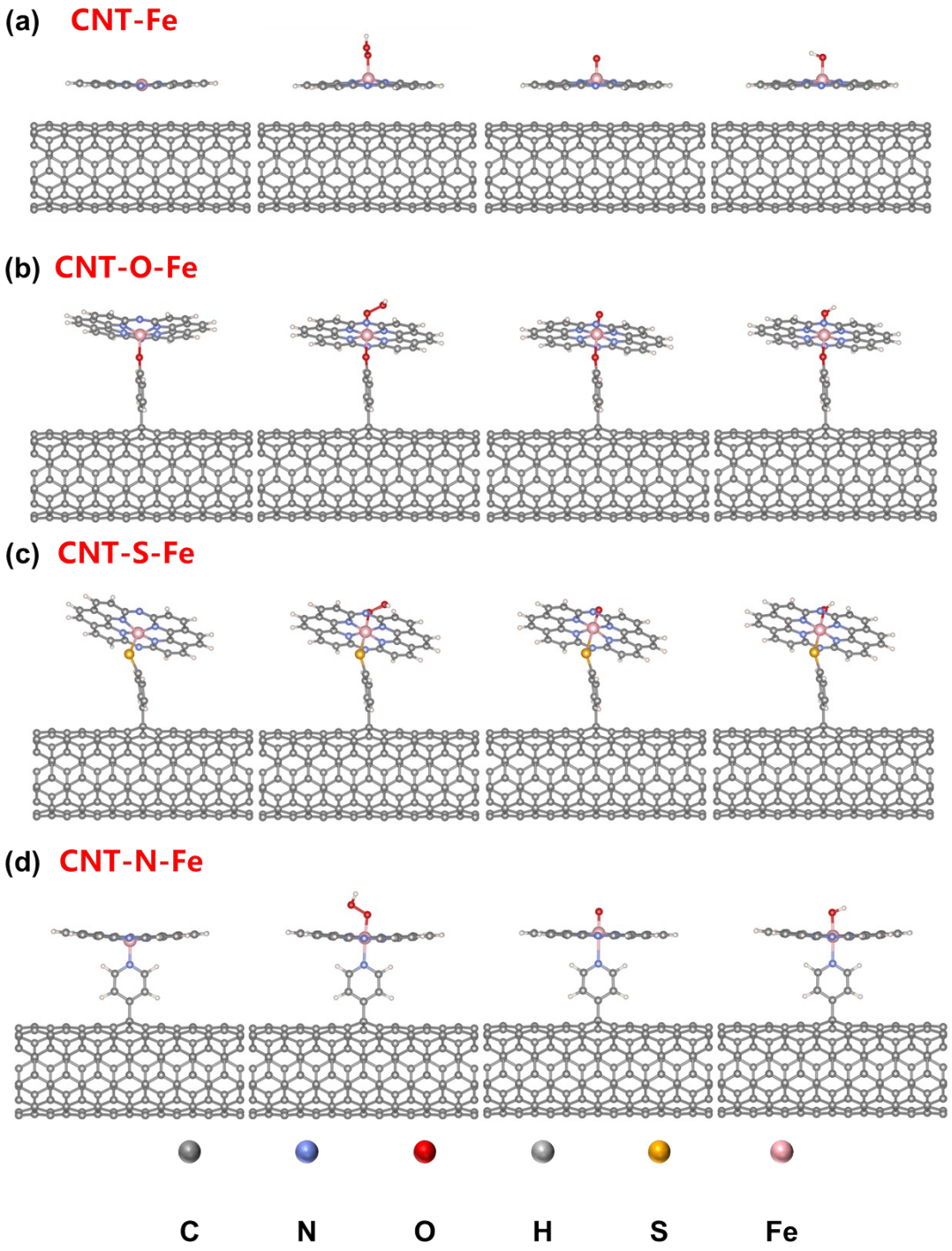

Figure S1. Side view of structure for (a) CNT-Fe, (b) CNT-O-Fe, (c) CNT-S-Fe, and (d) CNT-N-Fe adsorb *OOH, *O, *OH.

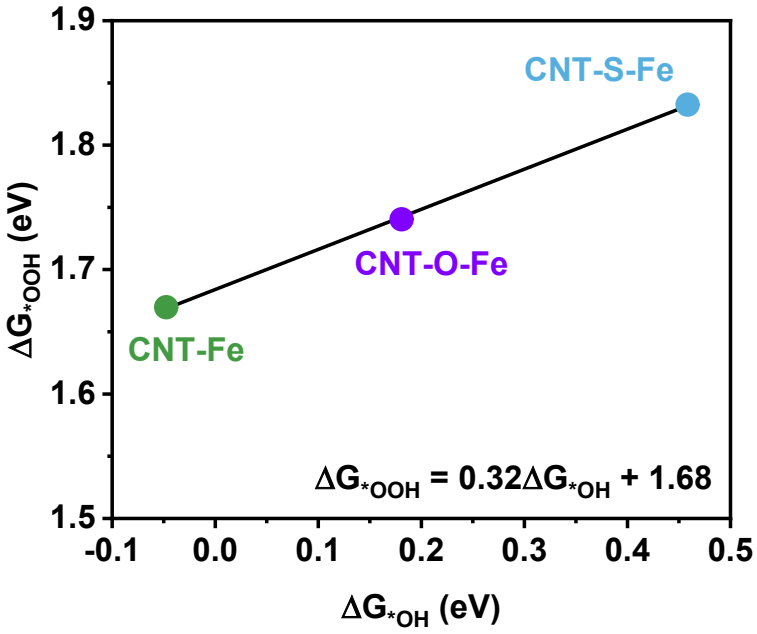

Figure S2. Linear relationship between ΔG_{*OOH} and ΔG_{*OH}.

The linear relationship between Gibbs free energies of *OOH intermediate (ΔG_{*OOH}) and *OH intermediate (ΔG_{*OH}) is calculated as follows:

$\Delta G_{*OOH} = 0.32\ \Delta G_{*OH} + 1.68$

The overpotential (η) for oxygen electroreduction can be calculated using the equation provided below:

$\eta = \max\ \{\Delta G_{*OOH} - 4.92, \Delta G_{*O} - \Delta G_{*OOH}, \Delta G_{*OH} - \Delta G_{*O}, -\Delta G_{*OH}\}/e + 0.46$

Given the linear correlation between ΔG_{*OOH} and ΔG_{*OH}, the equation above can be written as:

$\eta = \max\ \{0.3224\ \Delta G_{*OH} + 0.304, \Delta G_{*O} - 0.322\ \Delta G_{*OH} - 1.224, -\Delta G_{*O} + \Delta G_{*OH} + 0.46, -\Delta G_{*OH}\}/e$

Thereby, theoretical η can be related to only two Gibbs free energies descriptors: ΔG_{*OH} and $\Delta G_{*O} - \Delta G_{*OH}$.

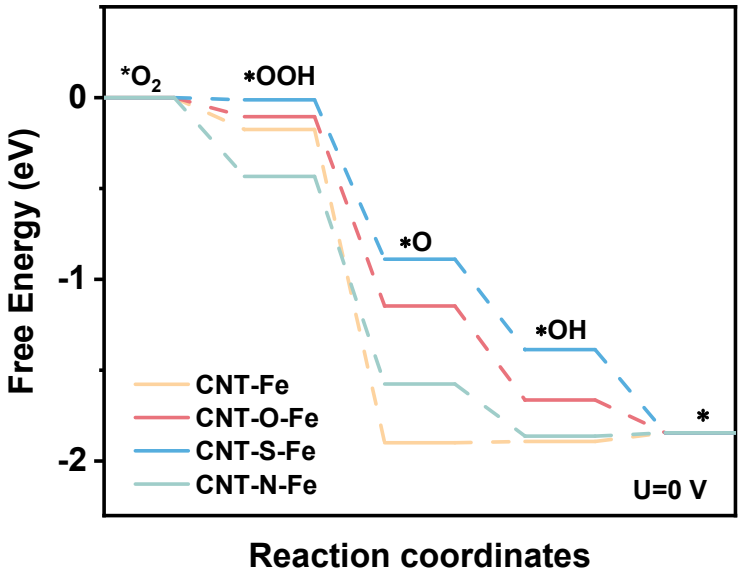

Figure S3. The Gibbs free energy diagram at U = 0 V for CNT-Fe, CNT-O-Fe, CNT-S-Fe, and CNT-N-Fe.

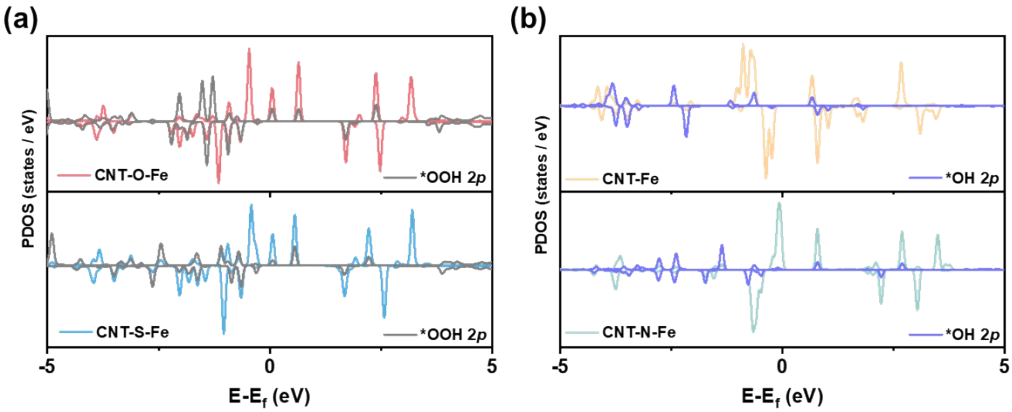

Figure S4. Projected density of states of Fe 3*d* and O 2*p* for (a) CNT-O-Fe and CNT-S-Fe, (b) CNT-Fe and CNT-N-Fe after oxygen intermediate formation.

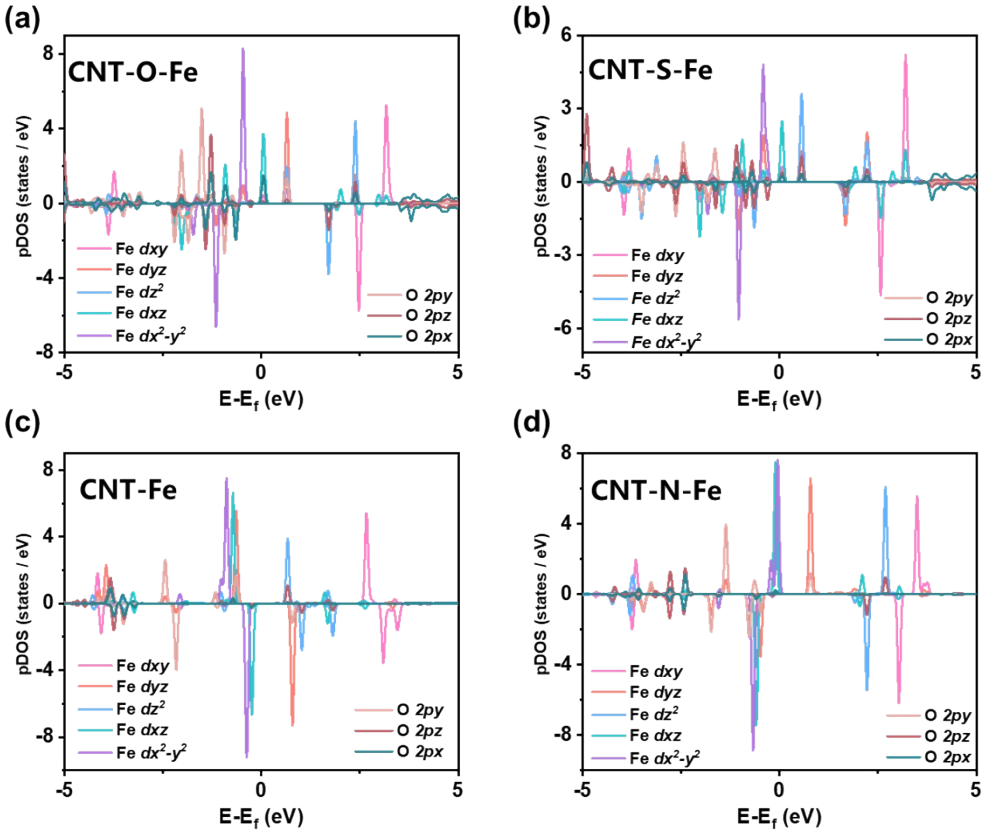

Figure S5. Projected density of states of Fe 3*d* and *OOH O 2*px*, 2*py*, 2*pz* of (a) CNT-O-Fe, (b) CNT-S-Fe, Fe 3*d* and *OH O 2*px*, 2*py*, 2*pz* of (c) CNT-Fe, (d) CNT-N-Fe.

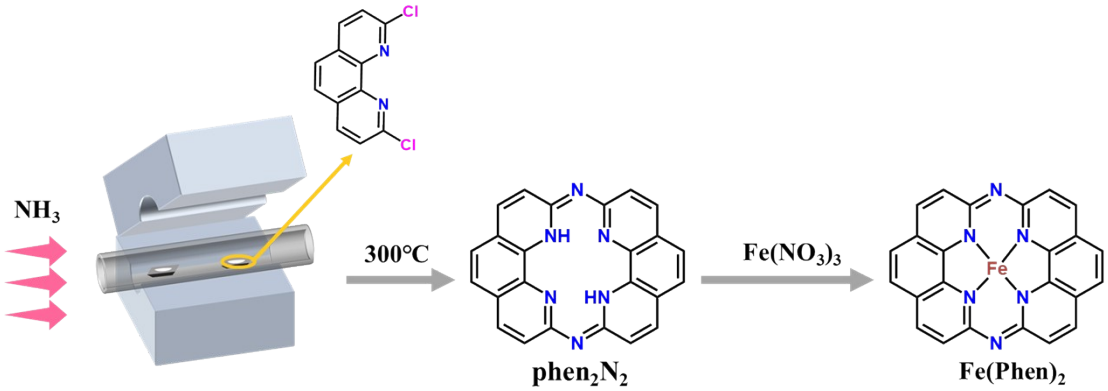

Figure S6. The schematic diagram for the synthesis of $phen_2N_2$ and $Fe(Phen)_2$.

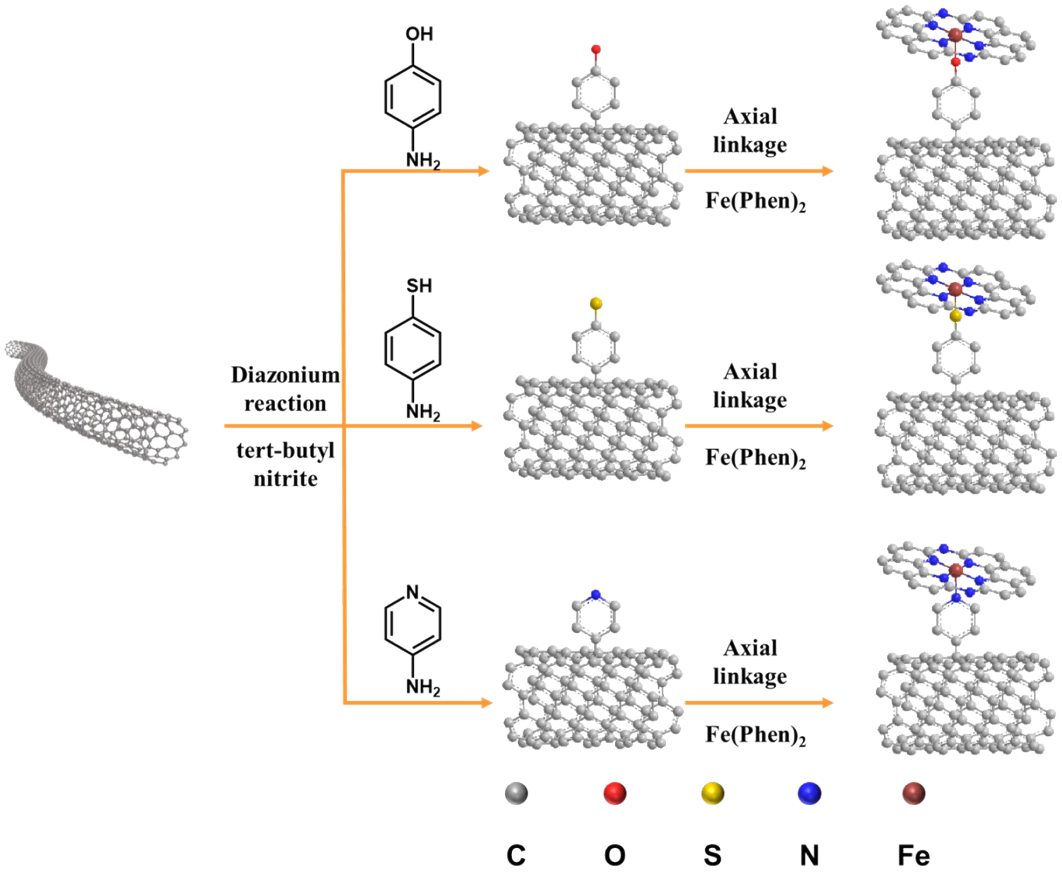

Figure S7. The schematic diagram for the synthesis of the $Fe(Phen)_2$ catalyst connecting on different functionalized CNT (CNT-X) through different electron bridge.

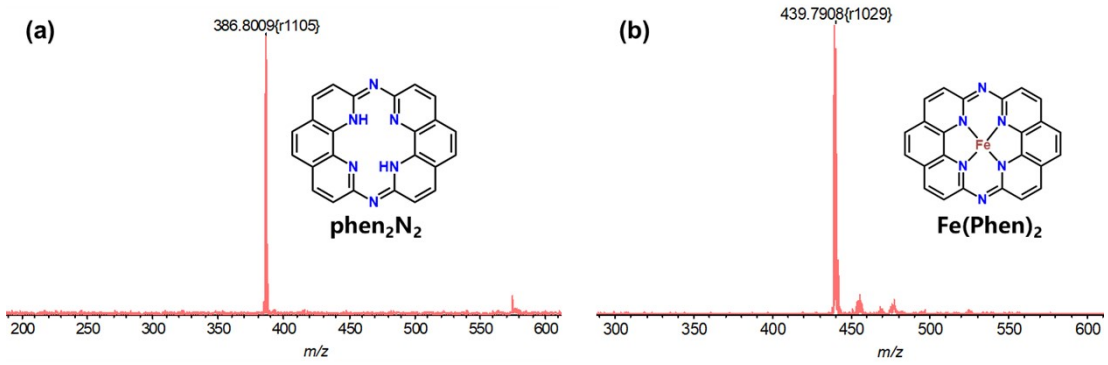

Figure S8. Time of flight mass spectrometry of (a) $phen_2N_2$ and (b) $Fe(Phen)_2$.

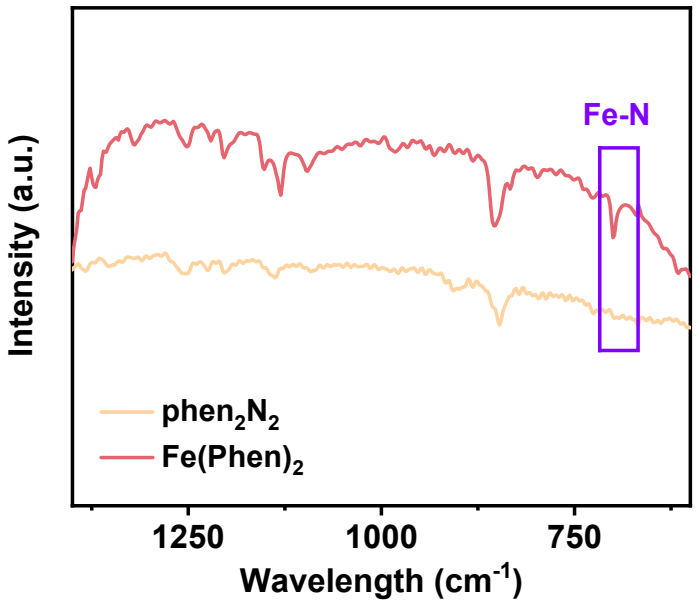

Figure S9. FT-IR spectra of $phen_2N_2$ and $Fe(Phen)_2$.

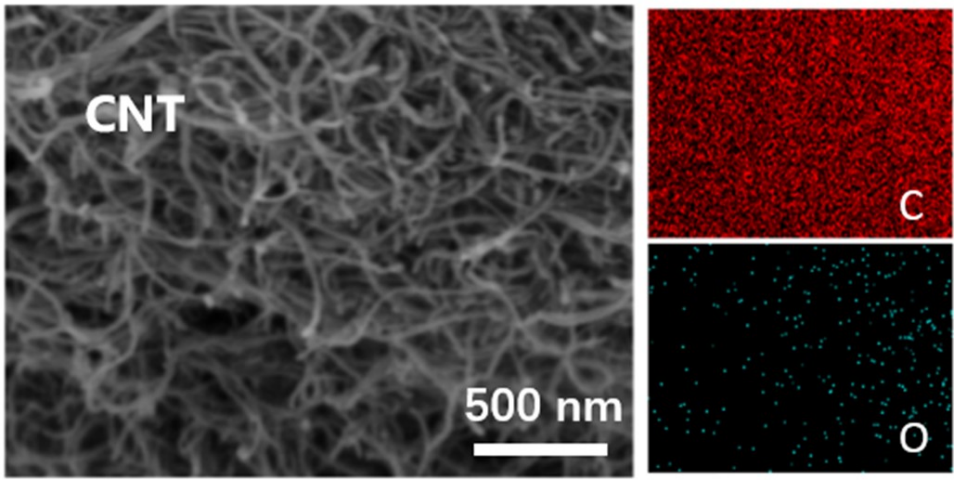

Figure S10. SEM image and corresponding EDS elemental mapping images of CNT.

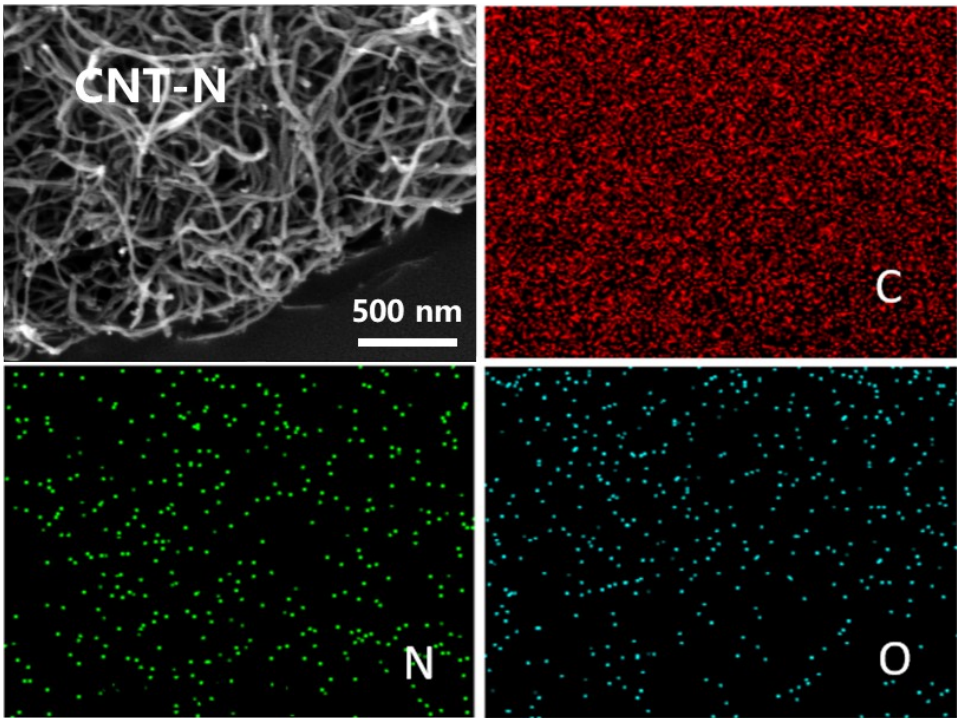

Figure S11. SEM image and corresponding EDS elemental mapping images of CNT-N.

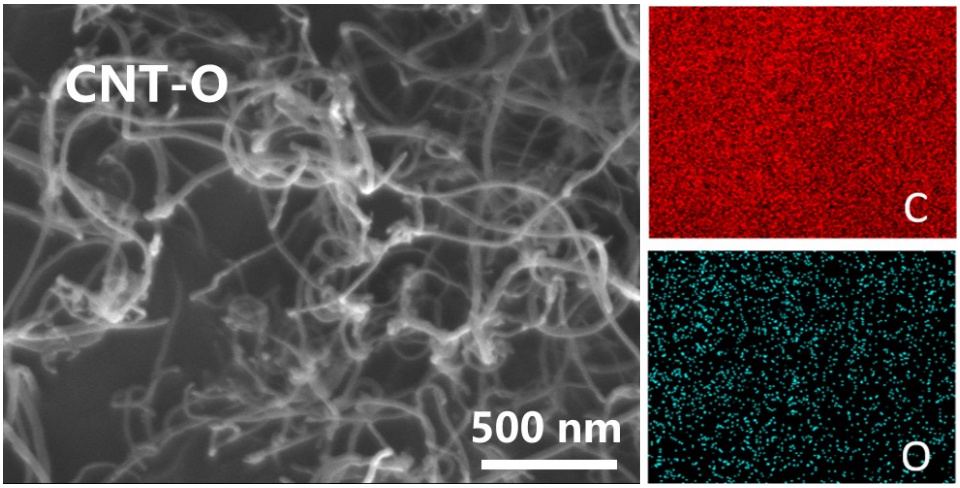

Figure S12. SEM image and corresponding EDS elemental mapping images of CNT-O.

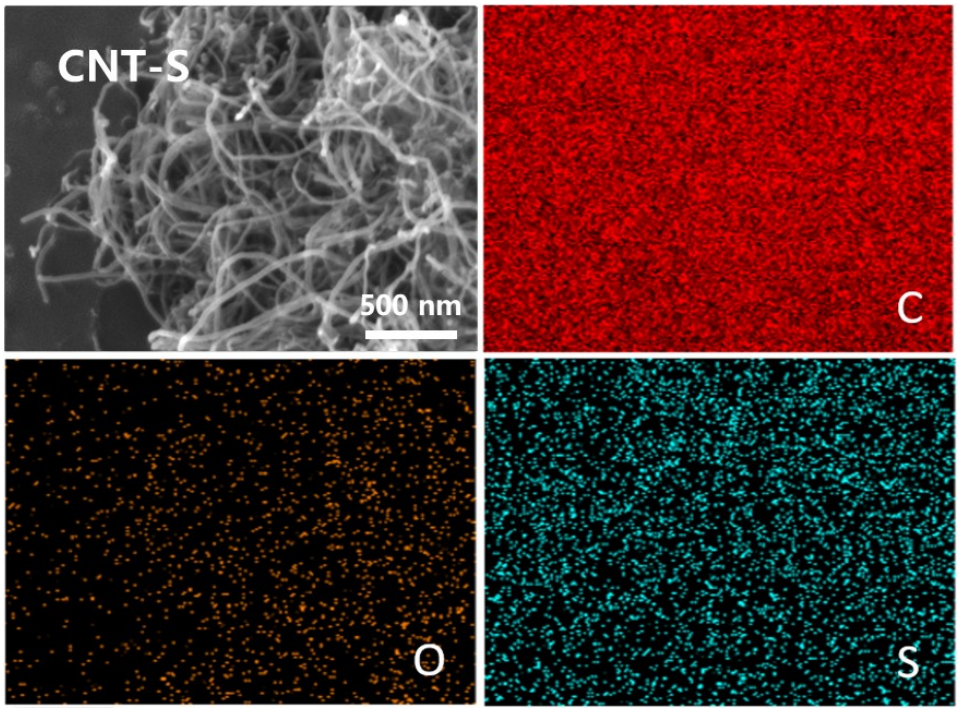

Figure S13. SEM image and corresponding EDS elemental mapping images of CNT-S.

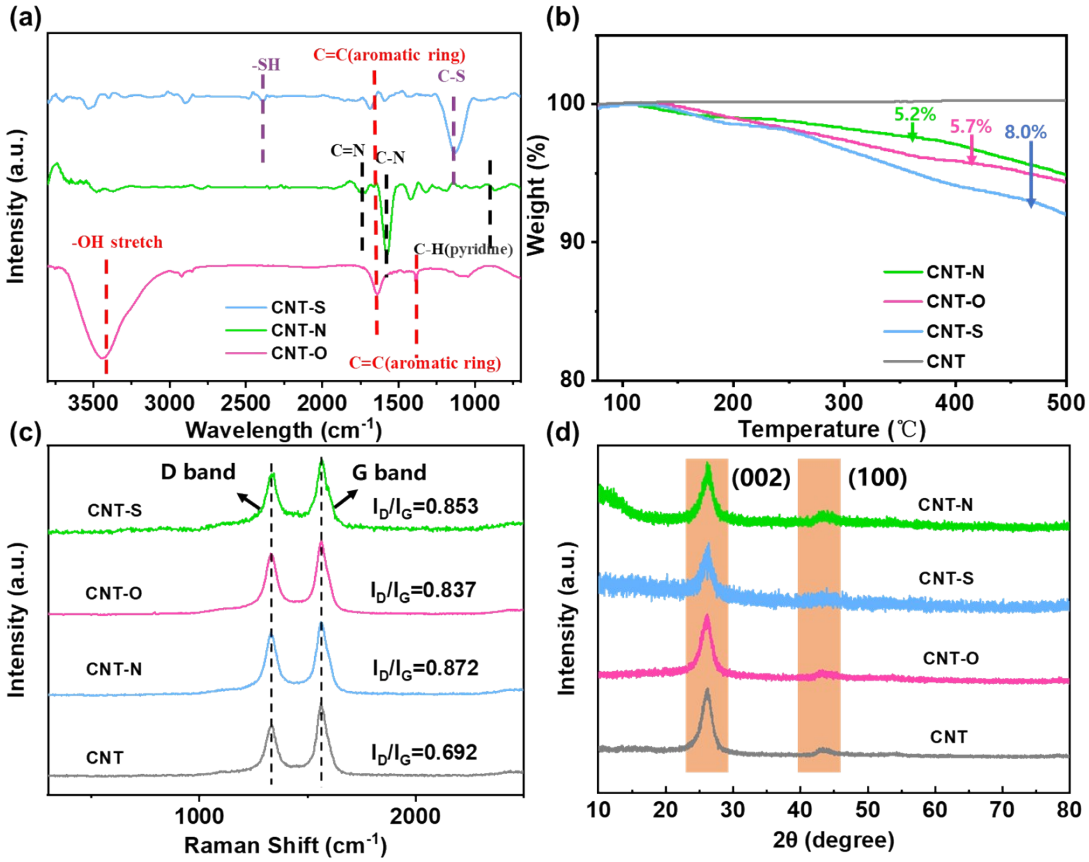

Figure S14. (a) FT-IR spectra, (b) TGA curves, (c) Raman spectra, (d) XRD pattern of CNT, CNT-N, CNT-O and CNT-S.

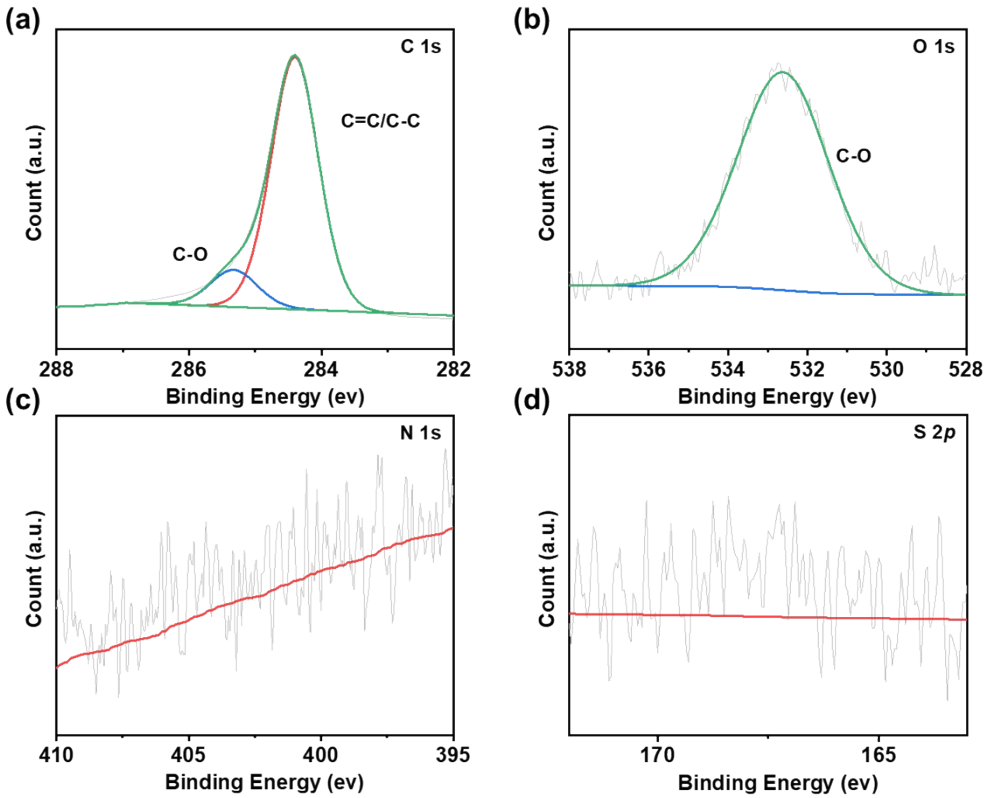

Figure S15. (a) C 1s XPS spectrum of CNT. (b.) O 1s XPS spectrum of CNT. (c) N 1s XPS spectrum of CNT. (d) S 2*p* XPS spectrum of CNT.

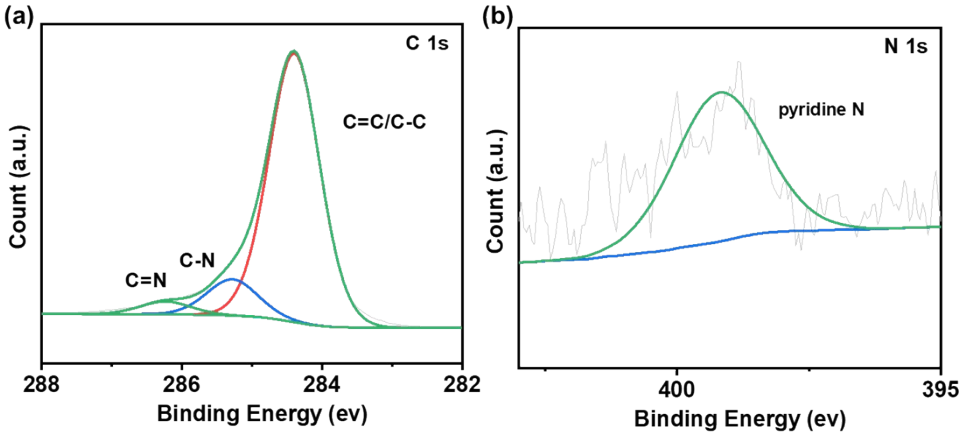

Figure S16. (a) C 1s XPS spectrum of CNT-N. (b) N 1s XPS spectrum of CNT-N.

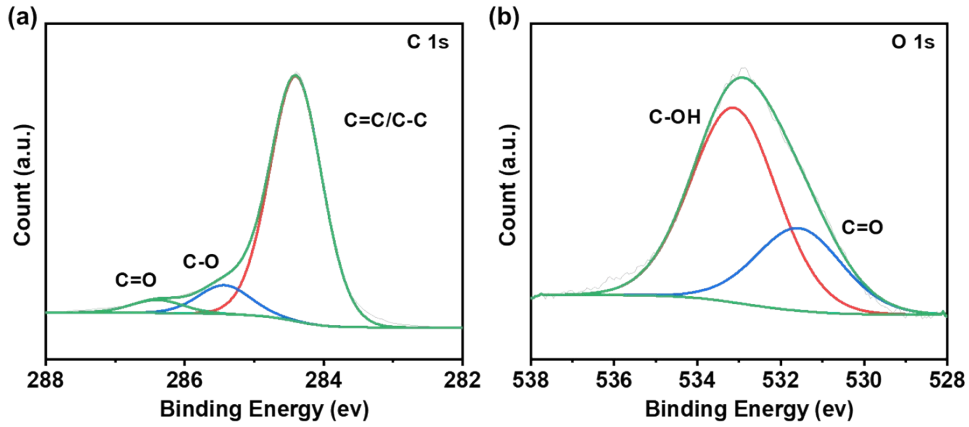

Figure S17. (a) C 1s XPS spectrum of CNT-O. (b) O 1s XPS spectrum of CNT-O.

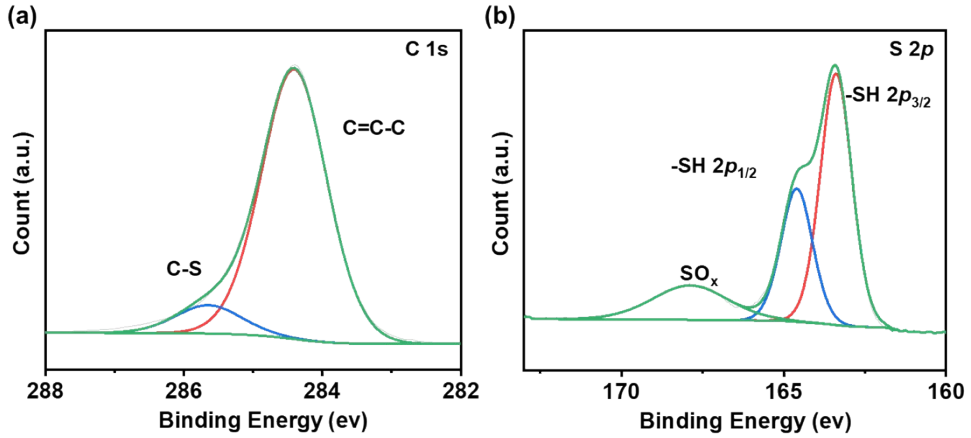

Figure S18. (a) C 1s XPS spectrum of CNT-S. (b) S 2*p* XPS spectrum of CNT-S.

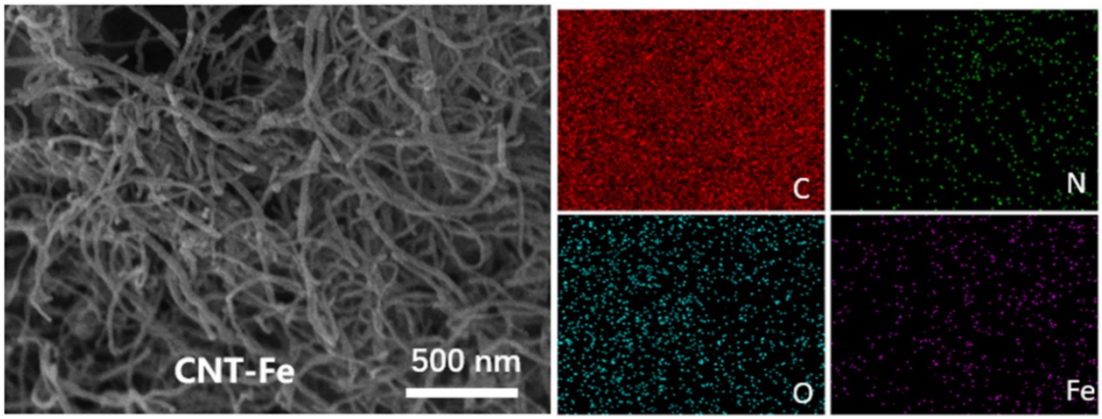

Figure S19. SEM image and corresponding EDS elemental mapping images of CNT-Fe.

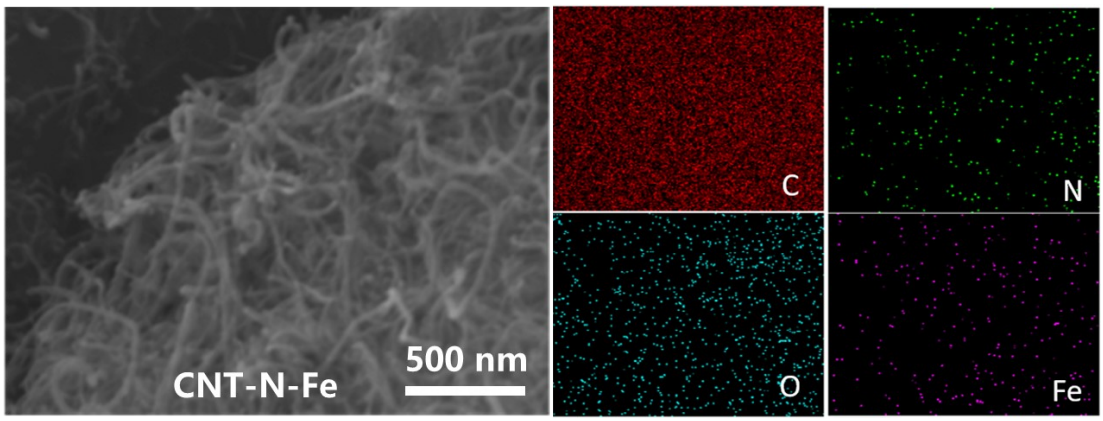

Figure S20. SEM image and corresponding EDS elemental mapping images of CNT-N-Fe.

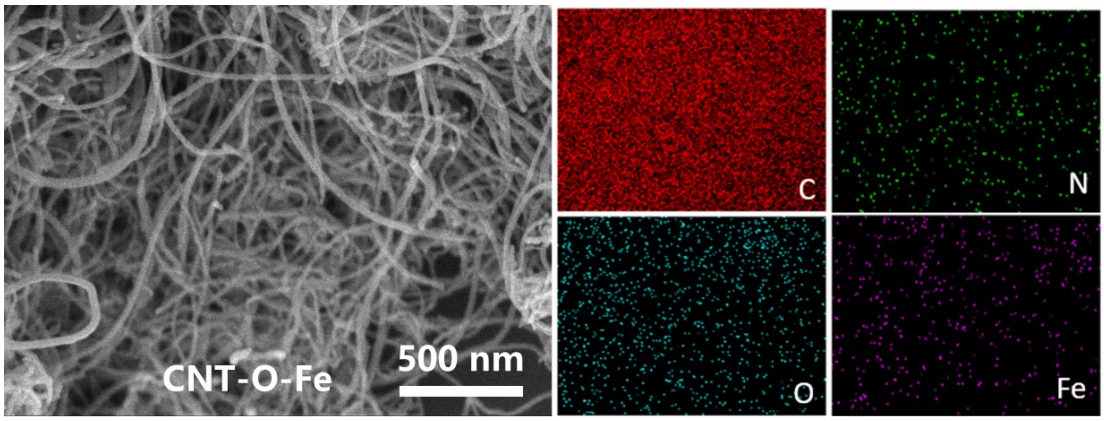

Figure S21. SEM image and corresponding EDS elemental mapping images of CNT-O-Fe.

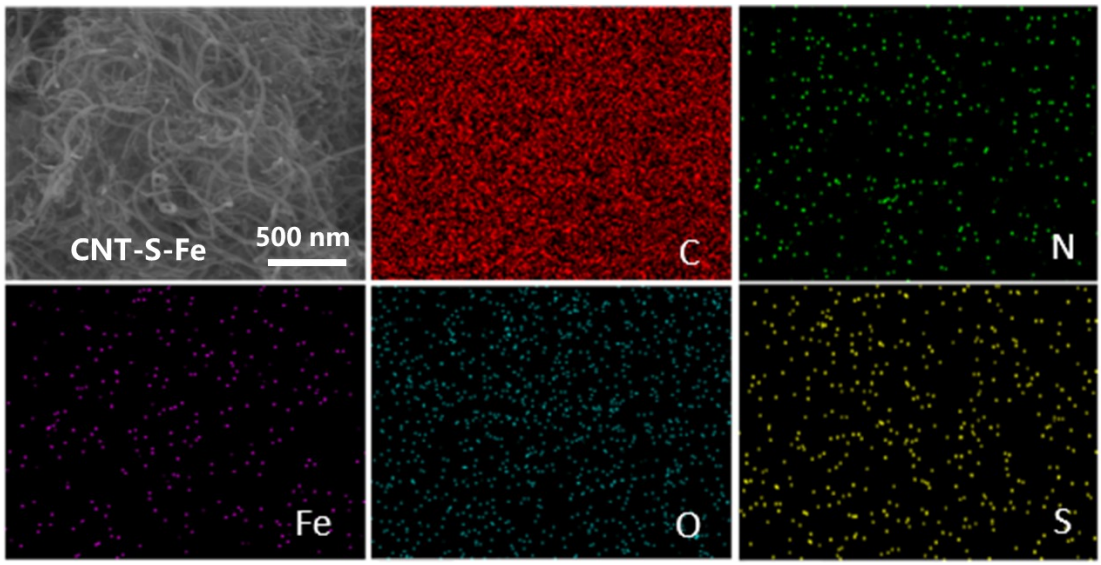

Figure S22. SEM image and corresponding EDS elemental mapping images of CNT-S-Fe.

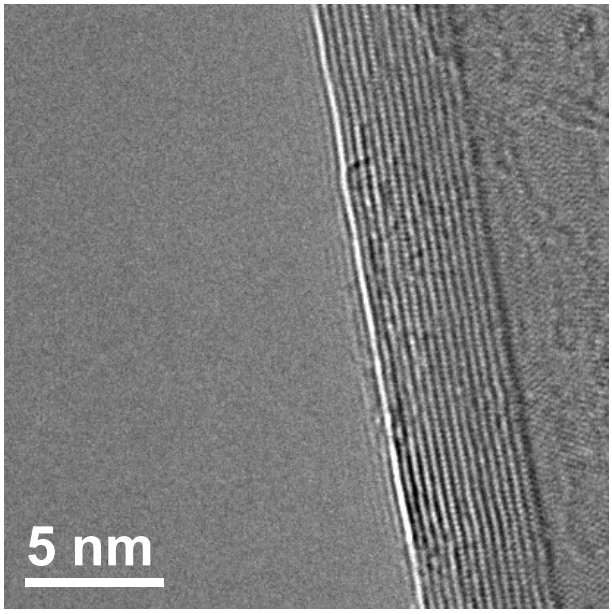

Figure S23. TEM image of CNT.

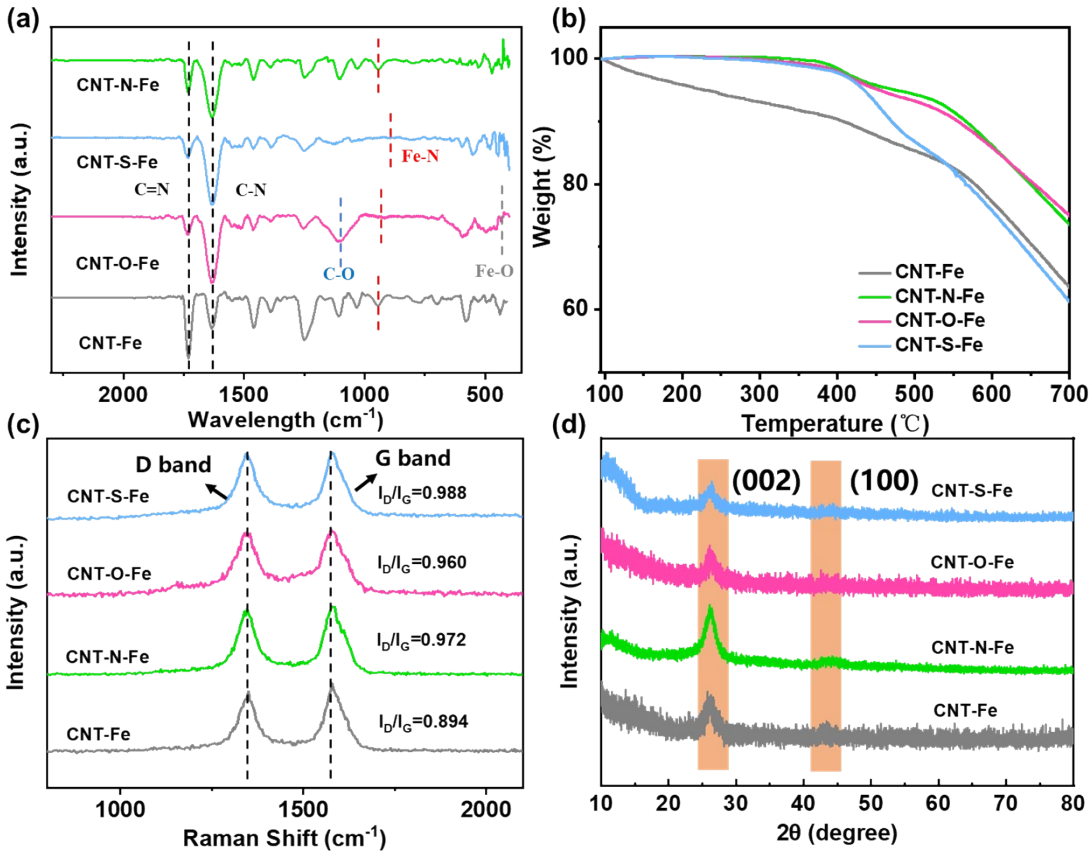

Figure S24. (a) FT-IR spectra, (b) TGA curves, (c) Raman spectra, and (d) XRD patterns of CNT-Fe, CNT-N-Fe, CNT-O-Fe and CNT-S-Fe.

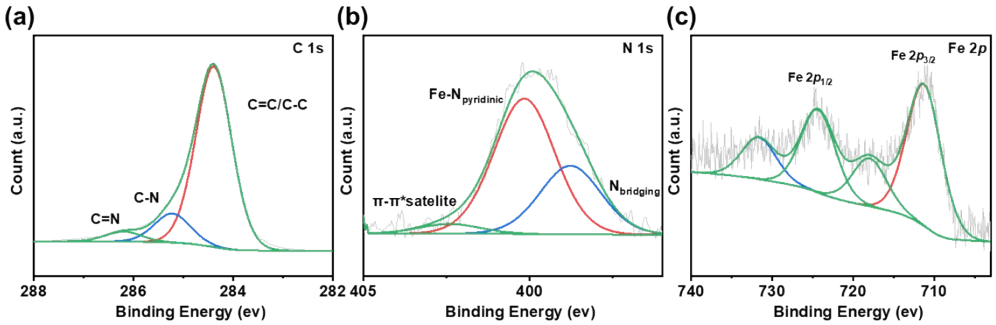

Figure S25. (a) C 1s XPS spectrum of CNT-Fe. (b) N 1s XPS spectrum of CNT-Fe. (c) Fe 2*p* XPS spectrum of CNT-Fe.

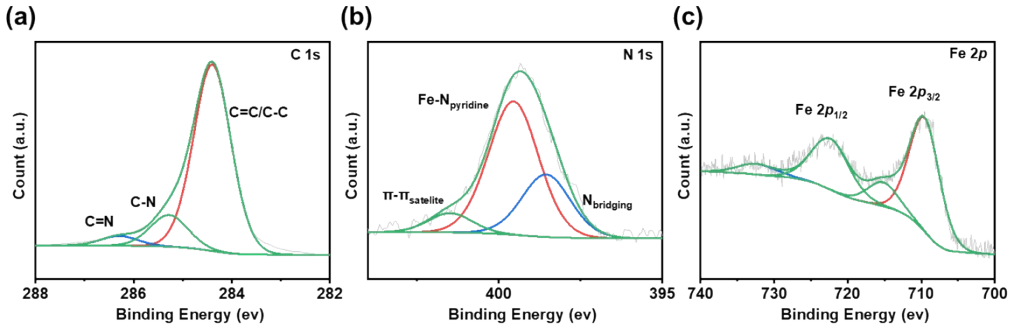

Figure S26. (a) C 1s XPS spectrum of CNT-N-Fe. (b) N 1s XPS spectrum of CNT-N-Fe. (c) Fe 2*p* XPS spectrum of CNT-N-Fe.

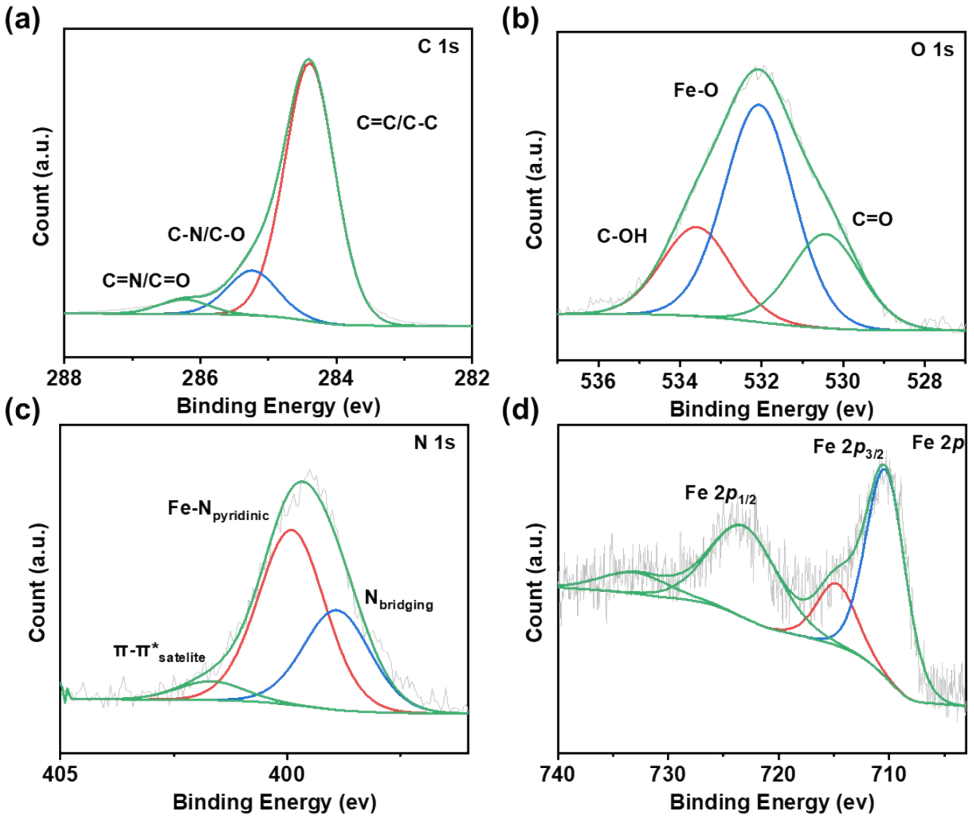

Figure S27. (a) C 1s XPS spectrum of CNT-O-Fe. (b) O 1s XPS spectrum of CNT-O-Fe. (c) N 1s XPS spectrum of CNT-O-Fe. (d) Fe 2*p* XPS spectrum of CNT-O-Fe.

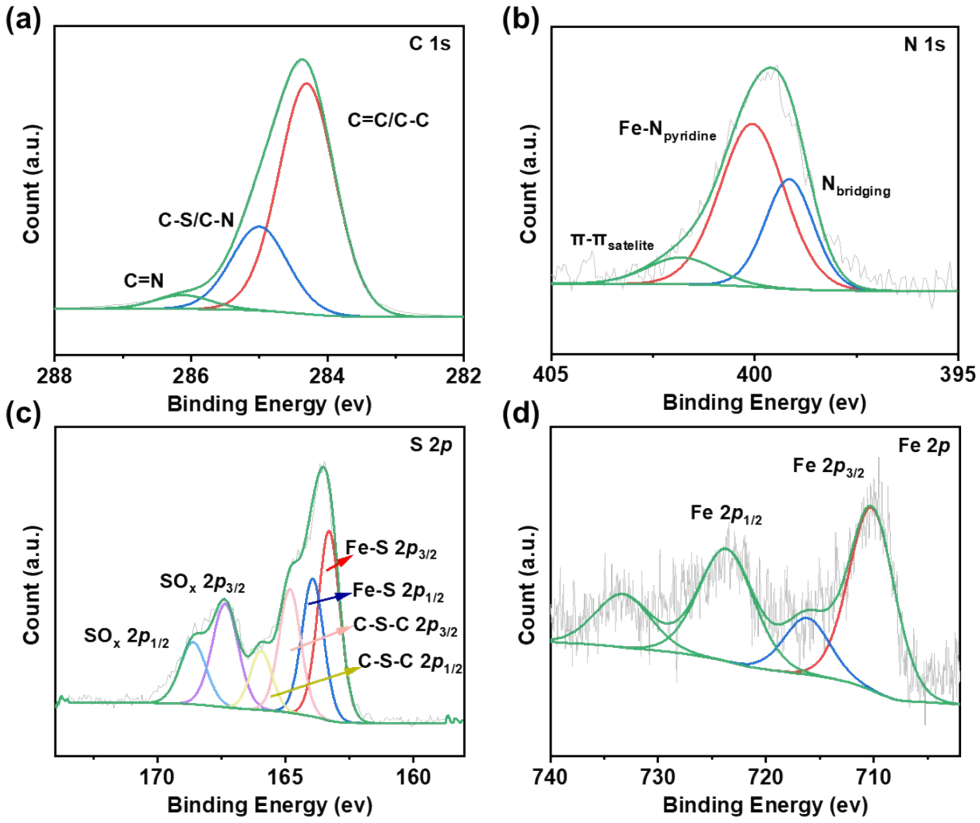

Figure S28. (a) C 1s XPS spectrum of CNT-S-Fe. (b) N 1s XPS spectrum of CNT-S-Fe. (c) S 2*p* XPS spectrum of CNT-S-Fe. (d) Fe 2*p* XPS spectrum of CNT-S-Fe.

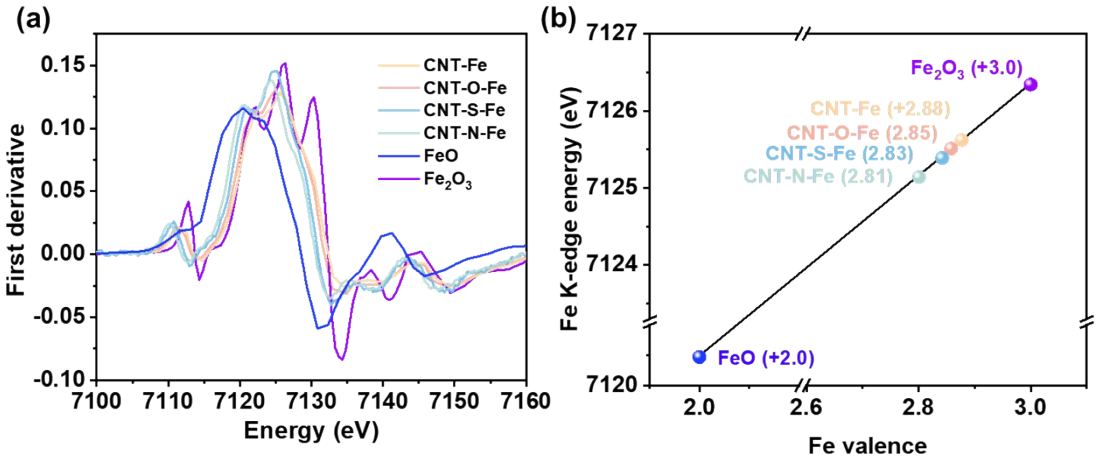

Figure S29. (a) The first derivative of Fe K-edge XANES for CNT-X-Fe, CNT-Fe, FeO, Fe_2O_3 and Fe foil. (b) Linear fitting curve of CNT-X-Fe, CNT-Fe, FeO and Fe_2O_3 derived from corresponding Fe K-edge XANES spectra.

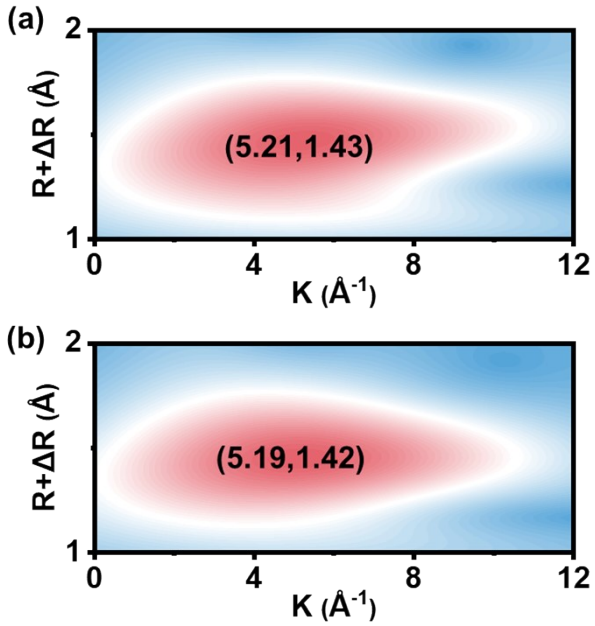

Figure S30. Wavelet transform of Fe K-edge EXAFS for (a) CNT-S-Fe and (b) CNT-N-Fe.

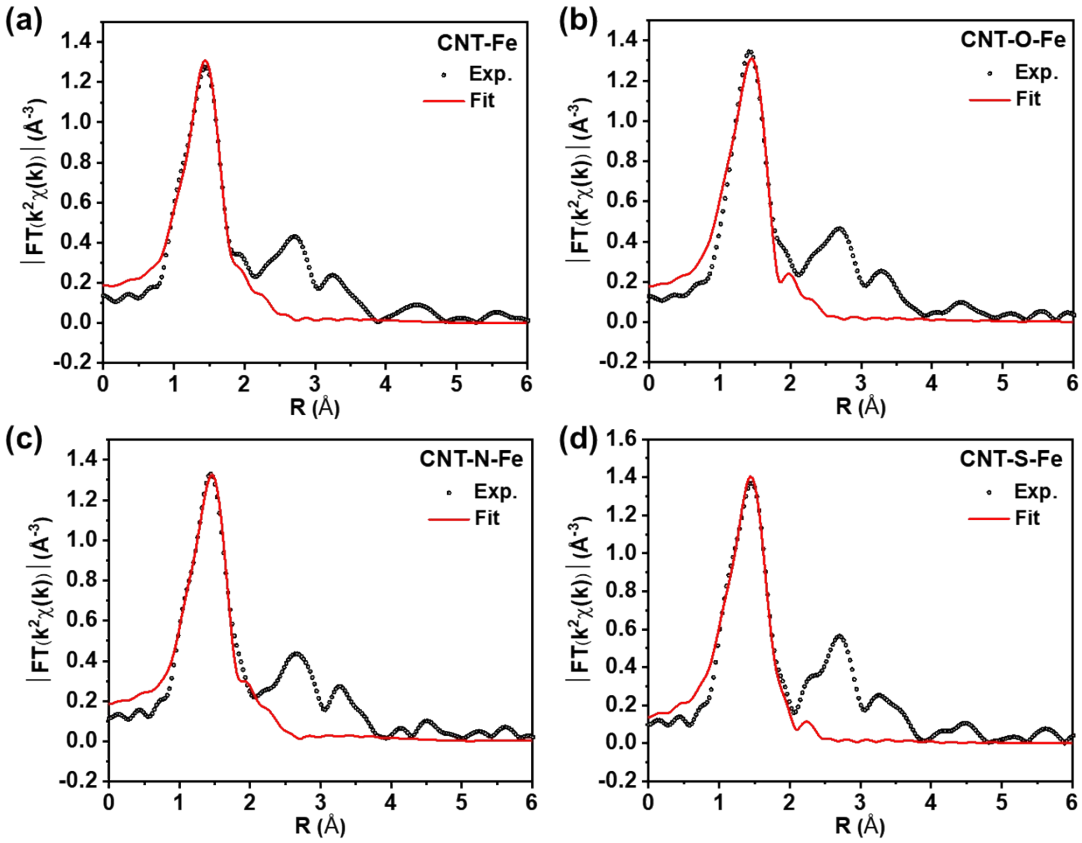

Figure S31. The Fourier transformations of the Fe K-edge EXAFS spectra and corresponding EXAFS R space fitting curves of (a) CNT-Fe, (b) CNT-O-Fe, (c) CNT-N-Fe, and (d) CNT-S-Fe.

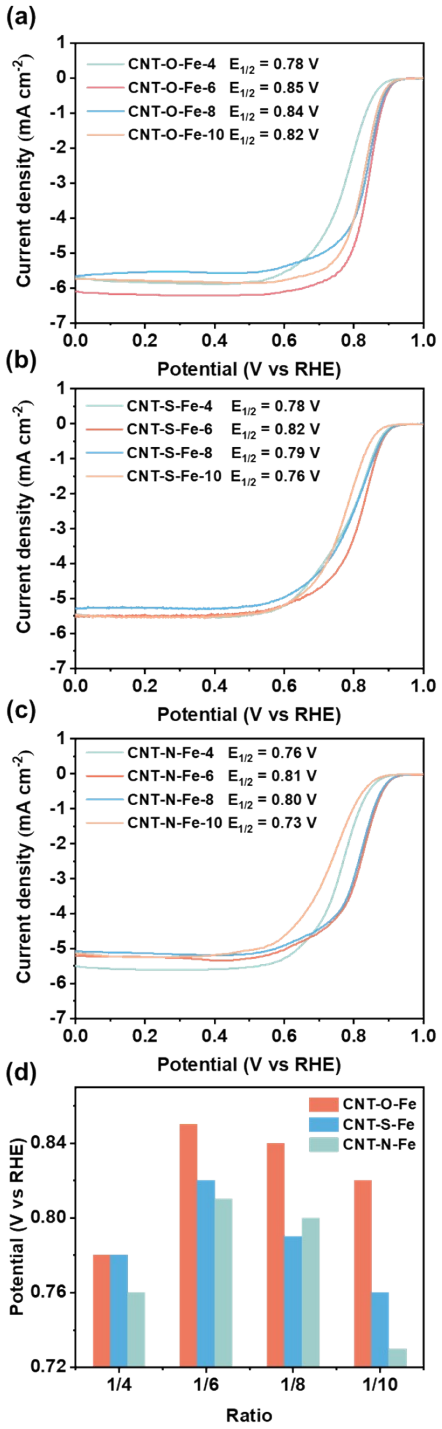

Figure S32. LSV polarization curves for oxygen reduction in O_2-saturated 0.1 M KOH for (a) CNT-O-Fe, (b) CNT-S-Fe and (c) CNT-N-Fe catalysts with different mass ratios of $Fe(Phen)_2$ to CNT-X (1:4, 1:6, 1:8, 1:10). (d) Column graph of $E_{1/2}$ with increasing ratio of $Fe(Phen)_2$ to CNT-X.

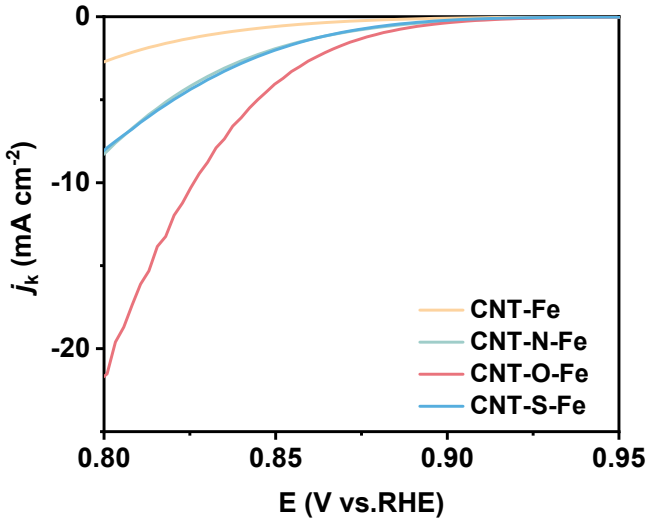

Figure S33. j_k (0.80 V vs. RHE) for CNT-O-Fe, CNT-S-Fe, CNT-N-Fe, and CNT-Fe.

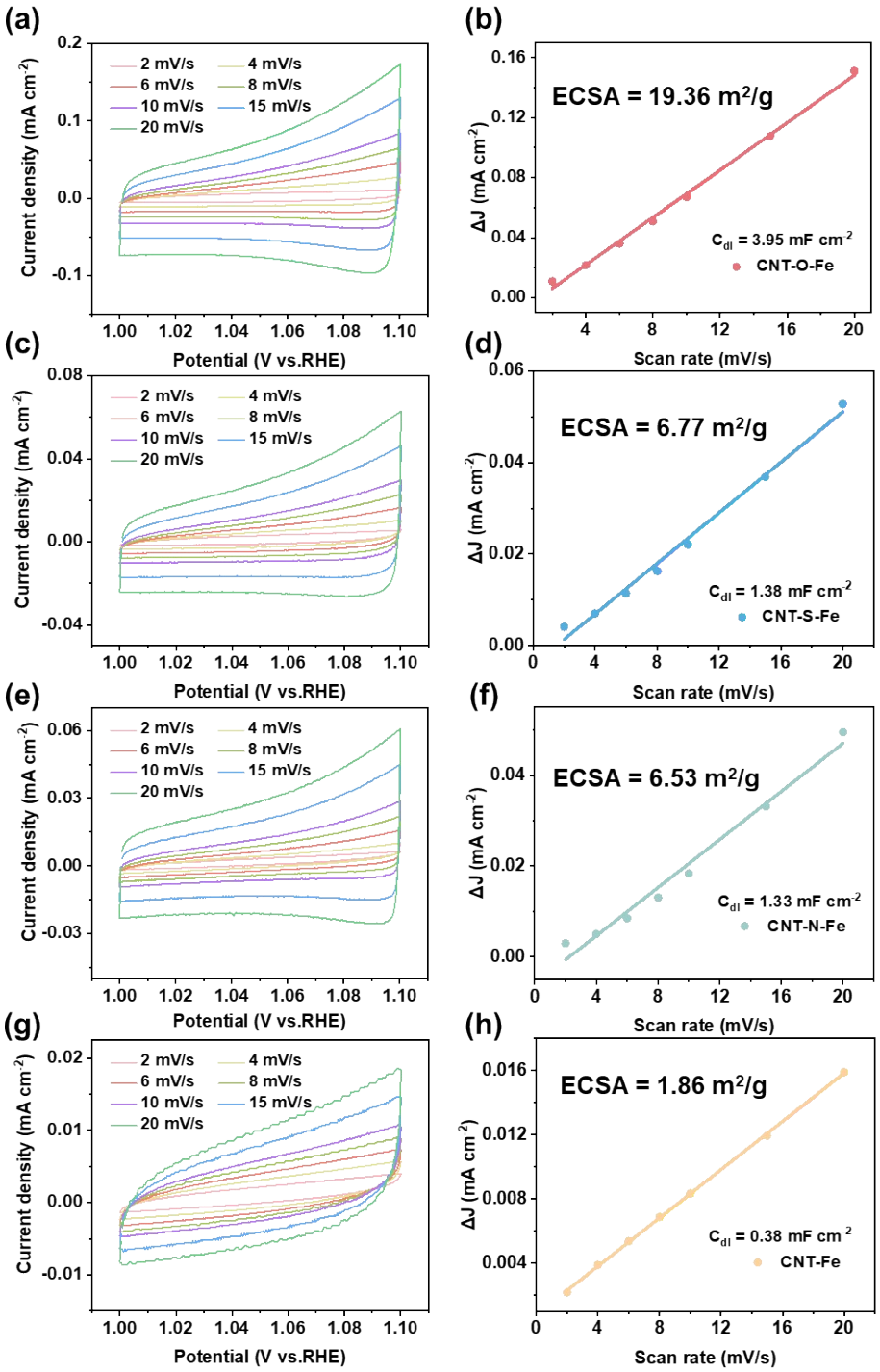

Figure S34. Cyclic voltammograms and corresponding double-layer capacitances (C_{dl}) of (a-b) CNT-O-Fe, (c-d) CNT-S-Fe, (e-f) CNT-N-Fe, and (g-h) CNT-Fe.

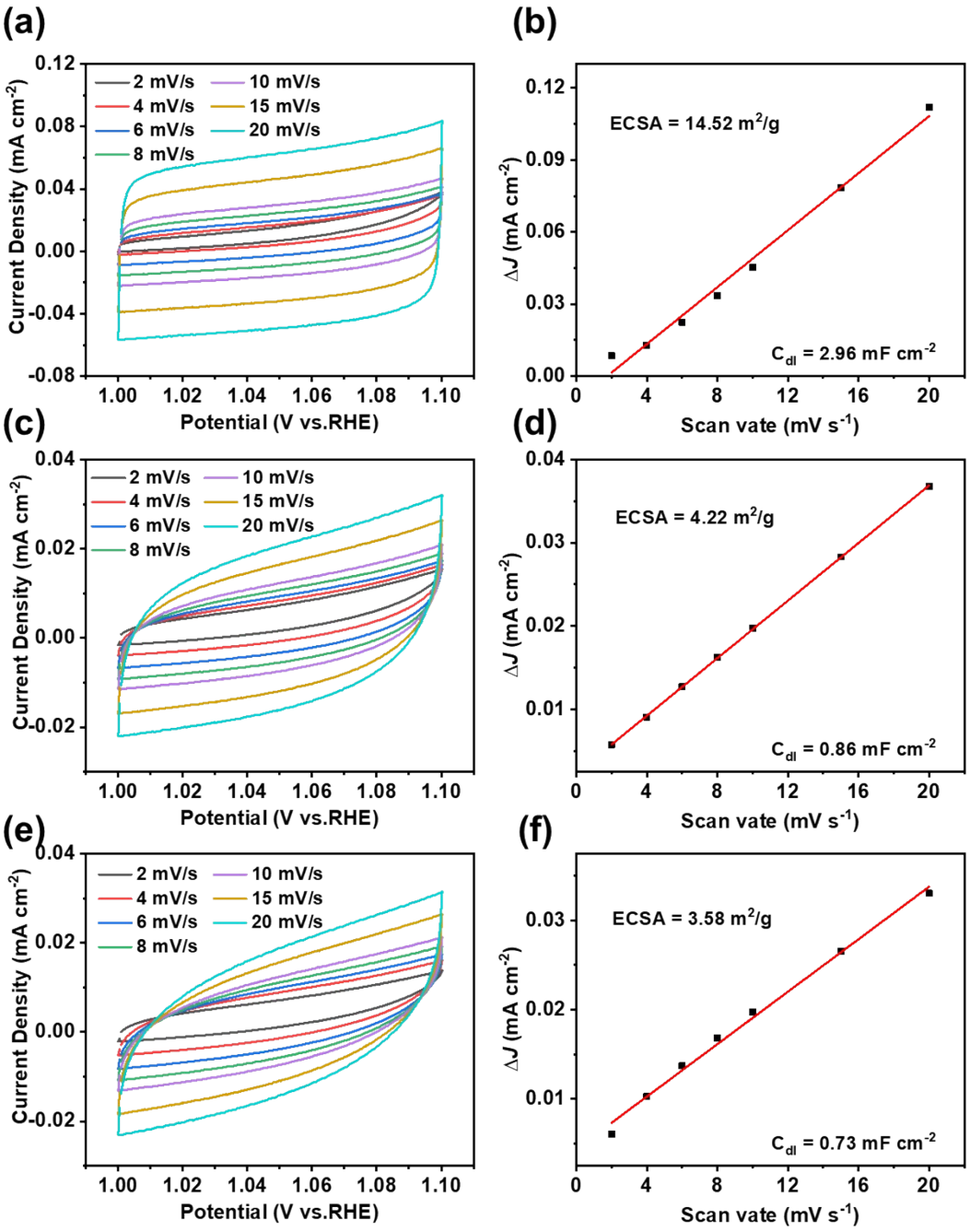

Figure S35. Cyclic voltammograms and corresponding double-layer capacitances (C_{dl}) of (a-b) CNT-O-Fe, (c-d) CNT-S-Fe, (e-f) CNT-N-Fe.

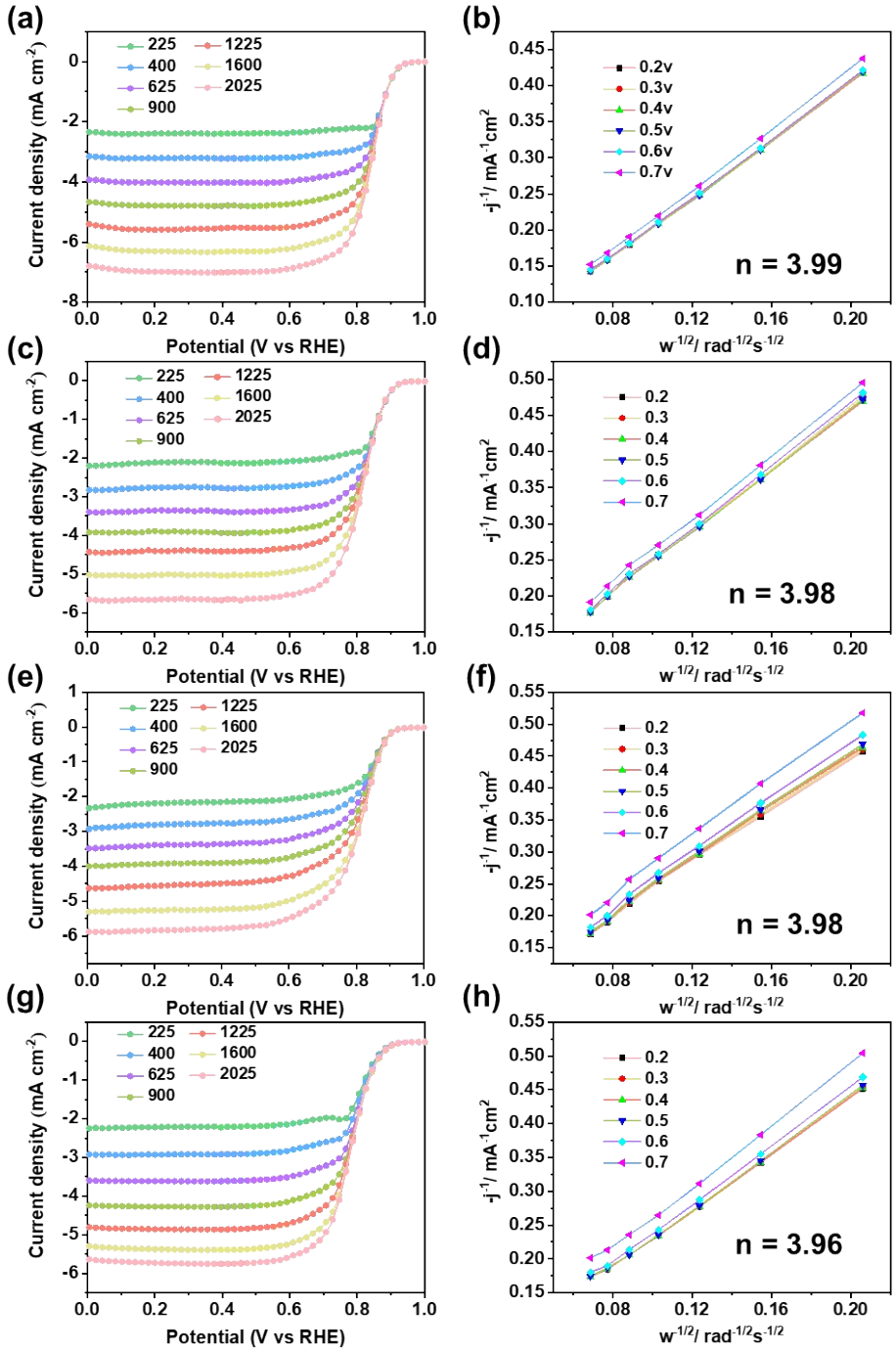

Figure S36. LSV curves at different rotation rates in O_2-saturated 0.1 M KOH and the corresponding Koutecky-Levich (K-L) plots of (a-b) CNT-O-Fe, (c-d) CNT-S-Fe, (e-f) CNT-N-Fe, and (g-h) CNT-Fe.

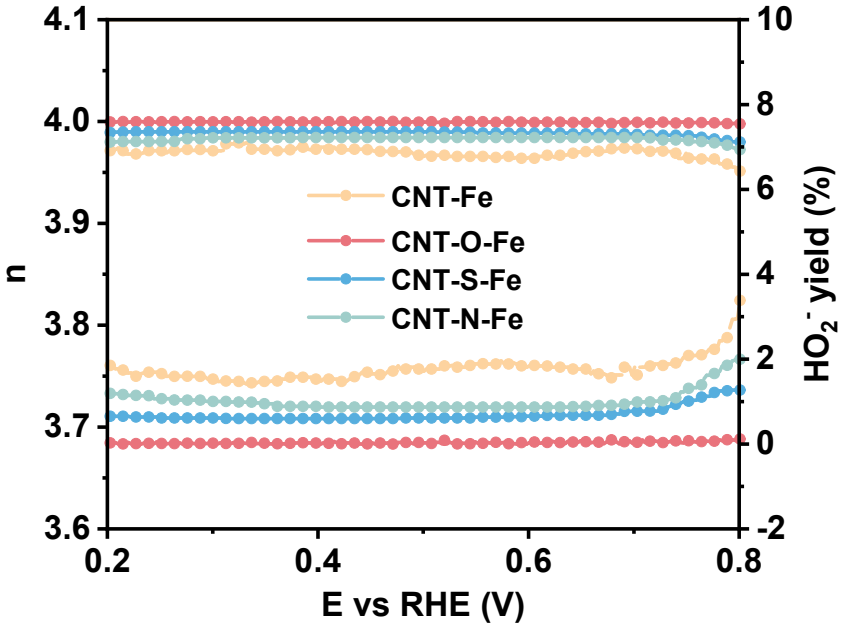

Figure S37. Electron transfer number (*n*) and HO_2^- yield for CNT-Fe and CNT-X-Fe.

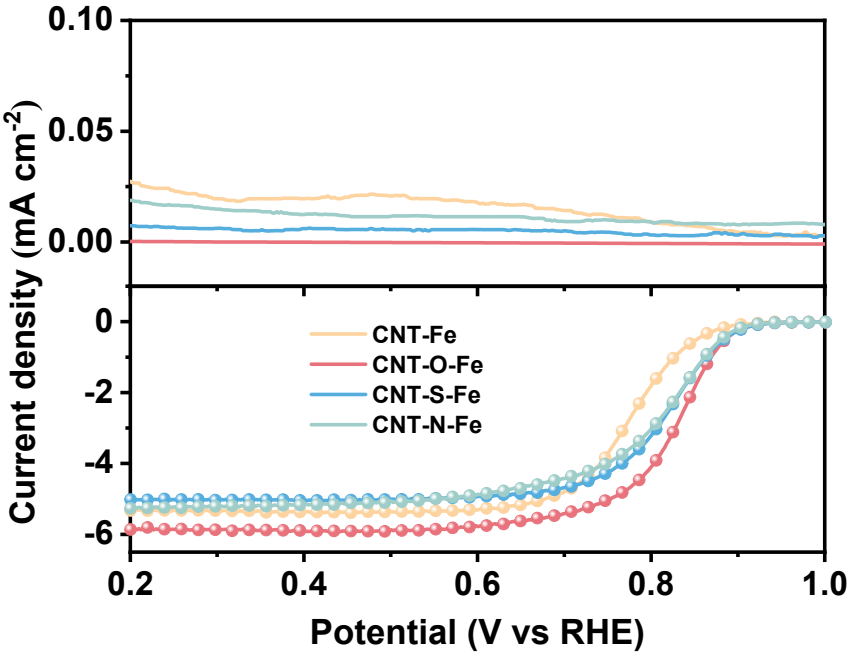

Figure S38. RRDE curves for CNT-Fe and CNT-X-Fe at a rotation speed of 1600.

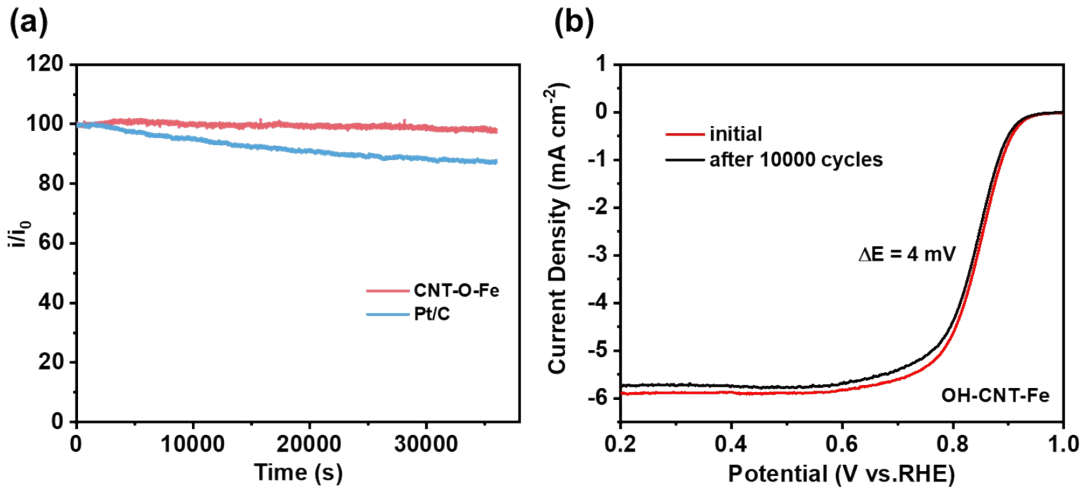

Figure S39. (a) Long time chronoamperometric response of CNT-O-Fe and Pt/C. (b) ORR polarization curves of CNT-O-Fe before and after 10000 cycles.

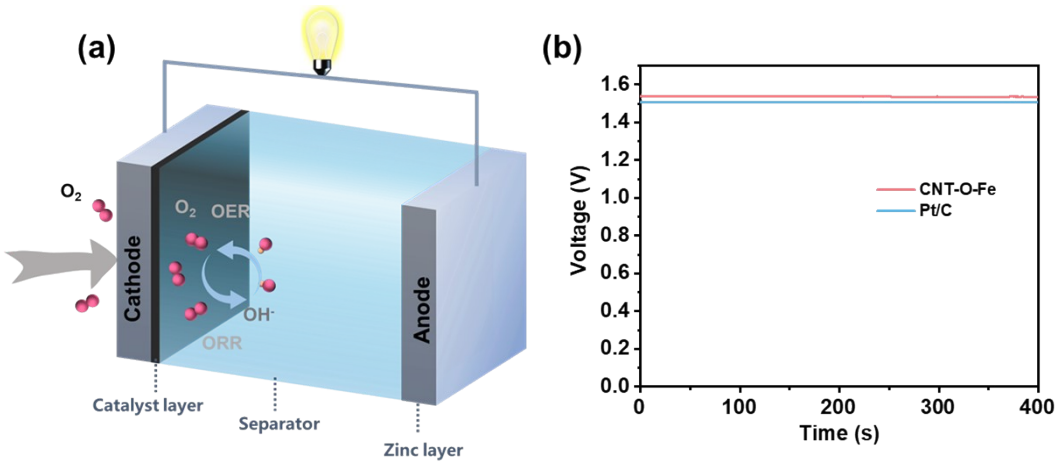

Figure S40. (a) Schematic illustration of the liquid ZAB configuration. (b) The open-circuit potential curves of CNT-O-Fe and Pt/C based ZABs.

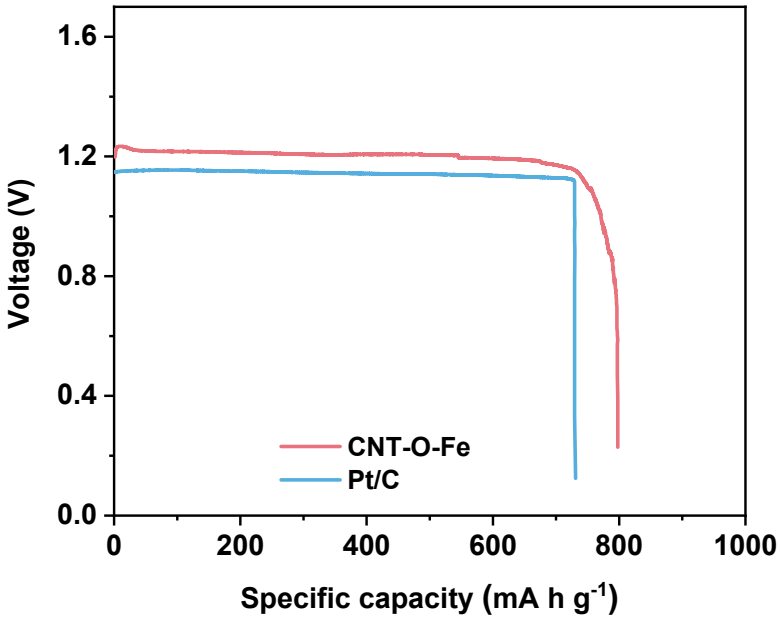

Figure S41. Long time galvanostatic discharge curves at 50 mA cm^{-2}.

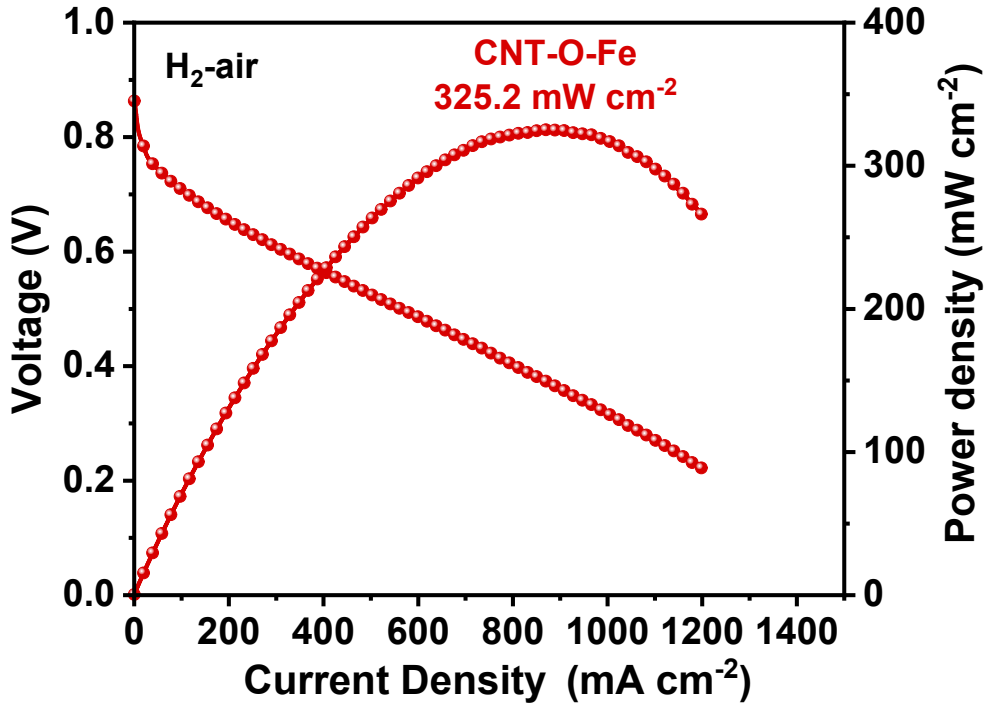

Figure S42. The cell voltage and power density plots for the CNT-O-Fe based anion exchange membrane fuel cell.

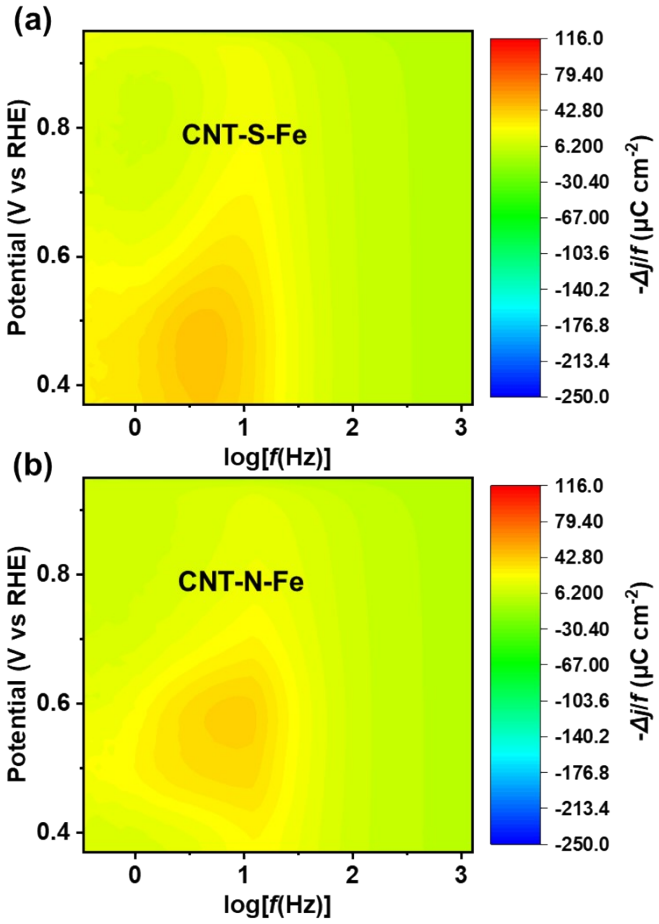

Figure S43. VF-SWV colormaps of (a) CNT-S-Fe and (b) CNT-N-Fe electrodes. Each graph is based on 54 square wave voltammograms collected in the frequency range from 0.33 to 1250 Hz.

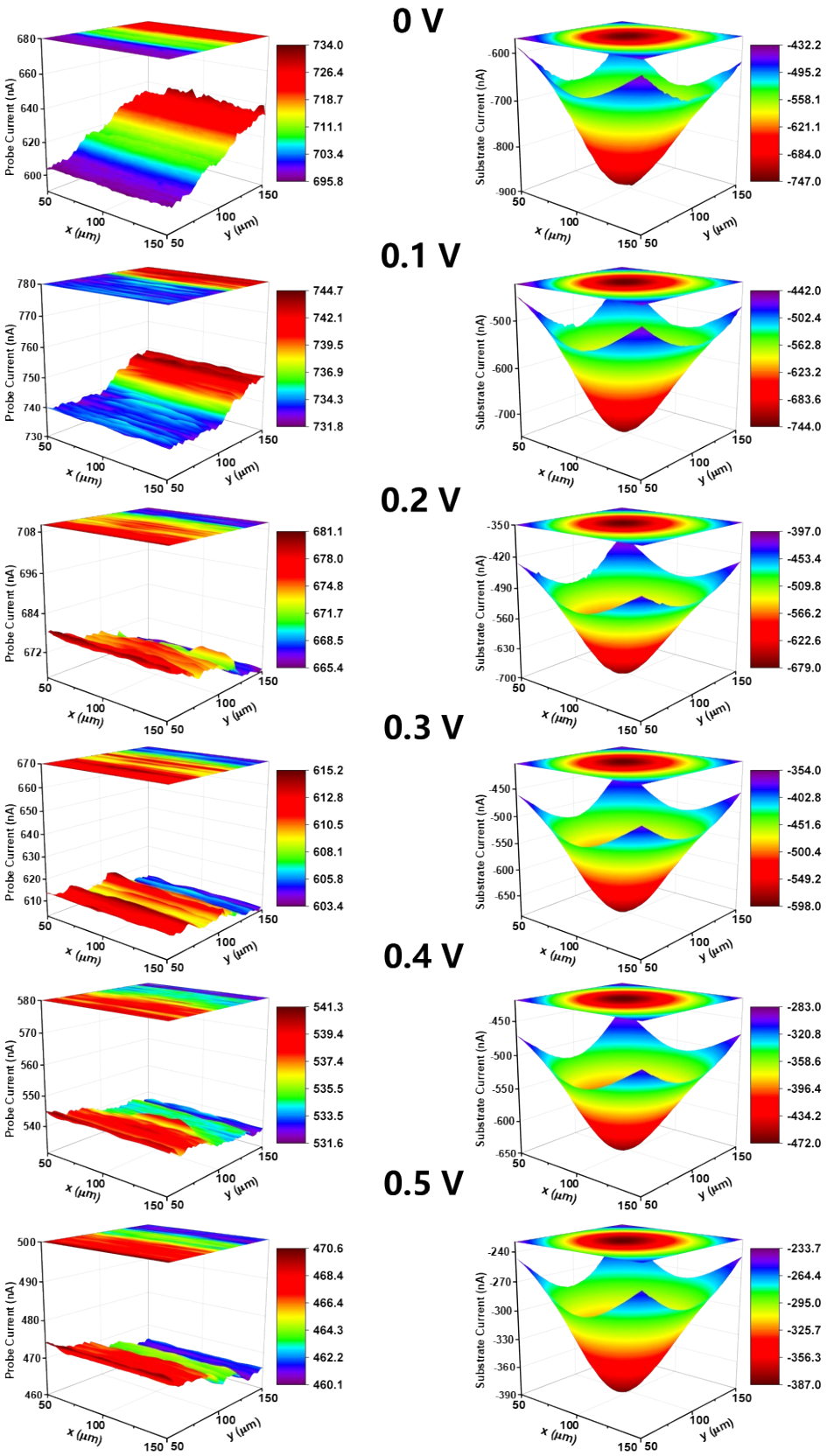

Figure S44. SECM images of CNT-O-Fe at substrate potential of 0.0 – 0.5 V (vs. RHE).

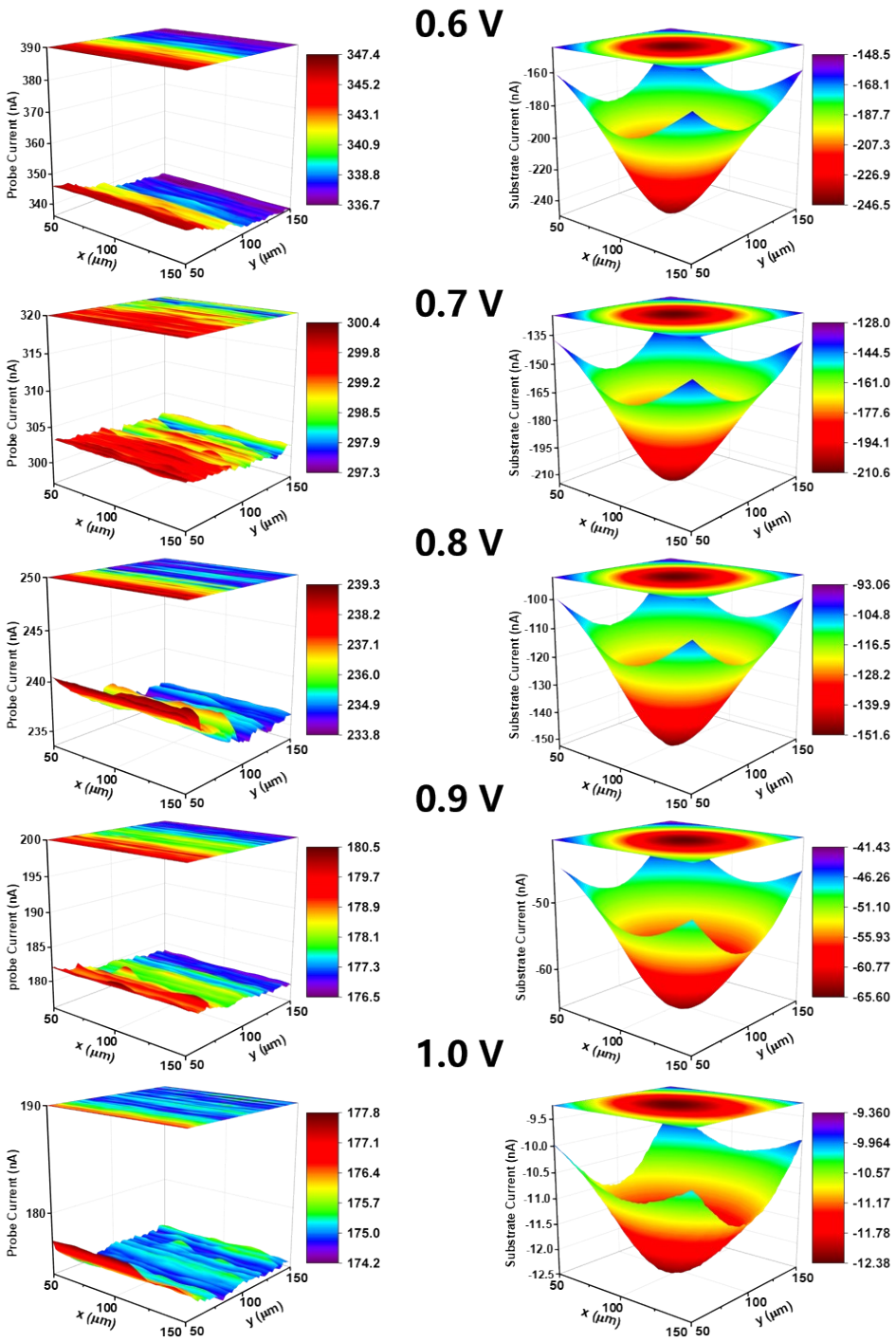

Figure S45. SECM images of CNT-O-Fe at substrate potential of 0.6 – 1.0 V (vs. RHE).

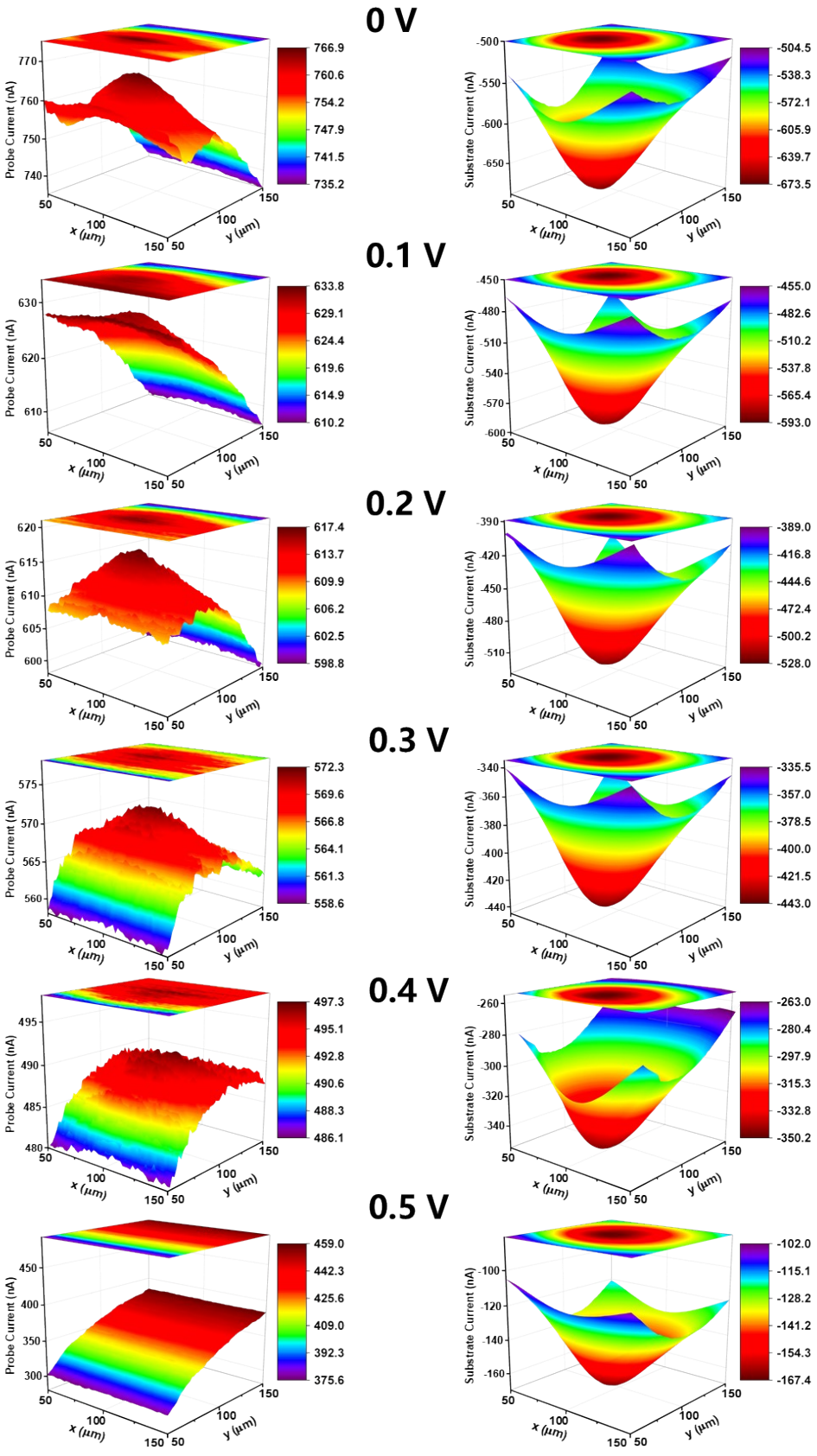

Figure S46. SECM images of CNT-S-Fe at substrate potential of 0.0 – 0.5 V (vs. RHE).

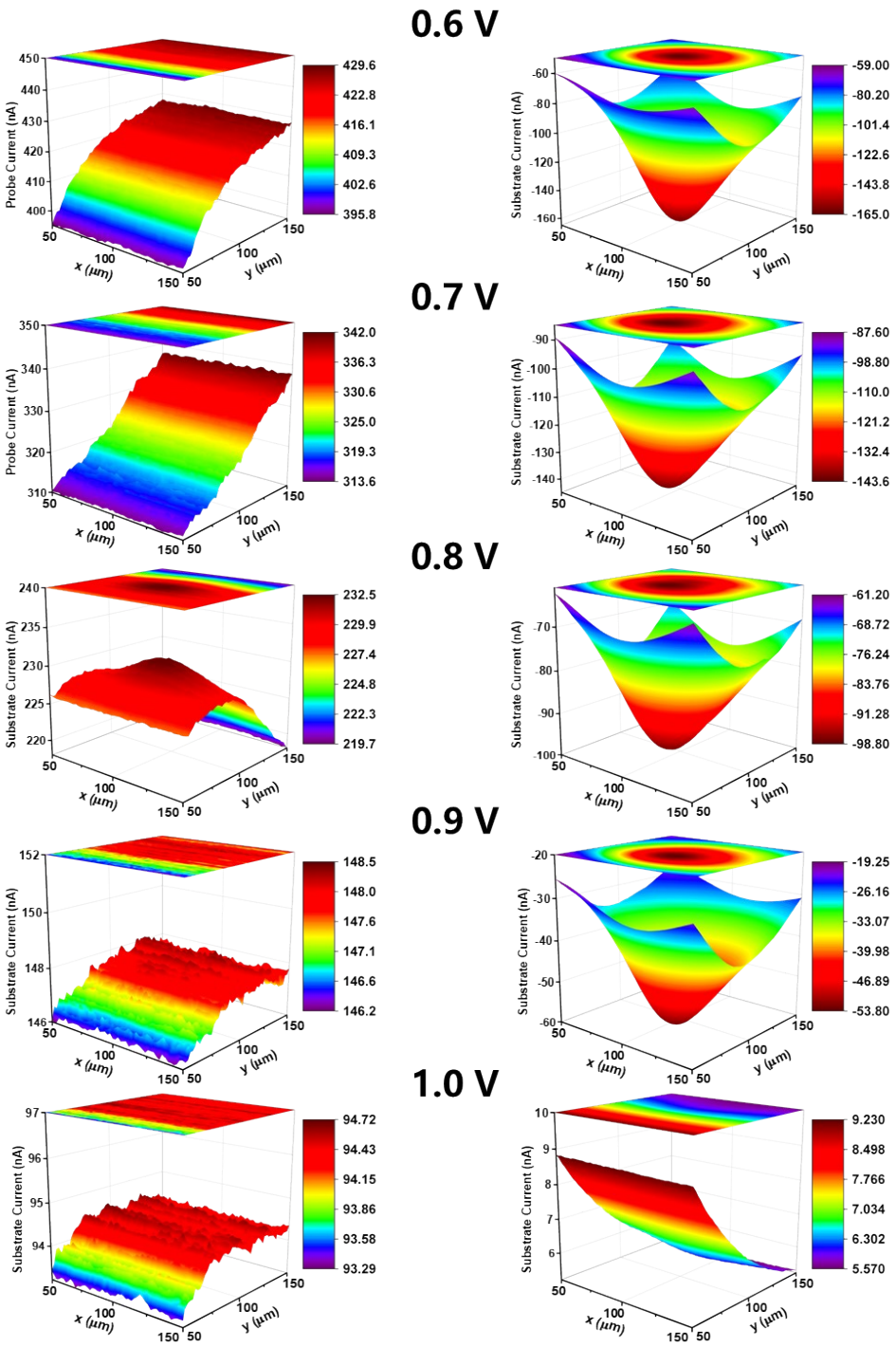

Figure S47. SECM images of CNT-S-Fe at substrate potential of 0.6 – 1.0 V (vs. RHE).

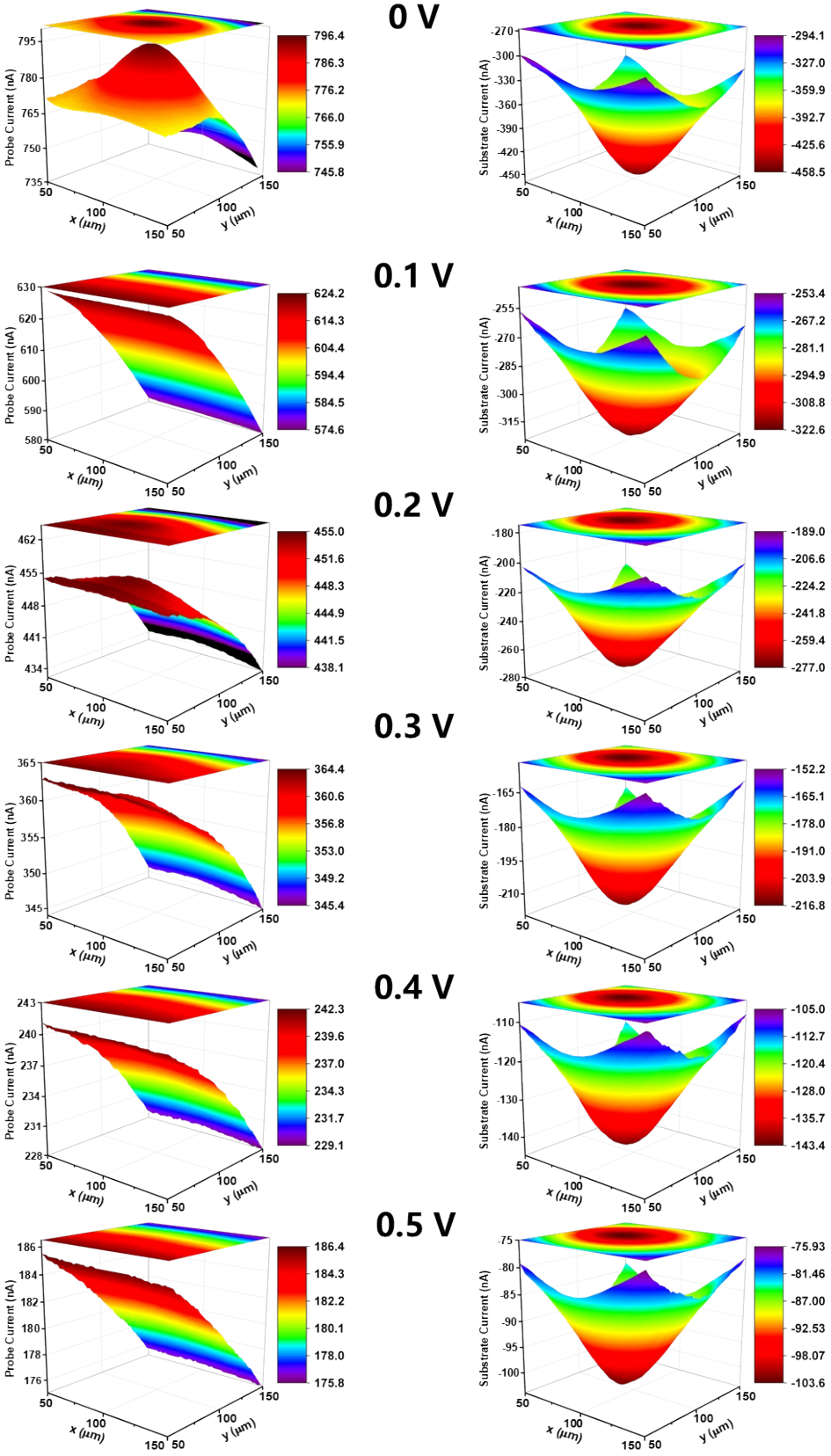

Figure S48. SECM images of CNT-N-Fe at substrate potential of 0.0 – 0.5 V (vs. RHE).

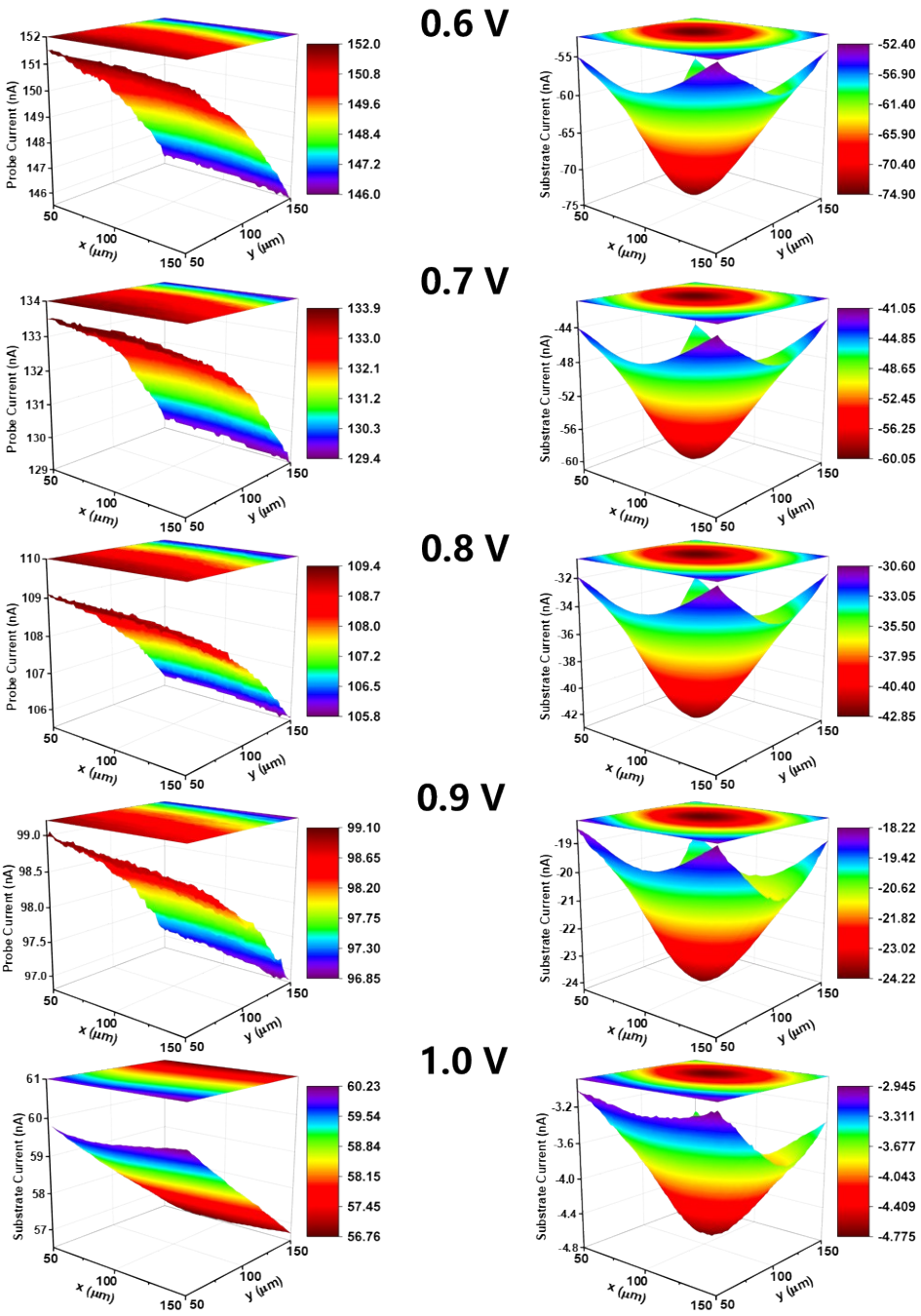

Figure S49. SECM images of CNT-N-Fe at substrate potential of 0.6 – 1.0 V (vs. RHE).

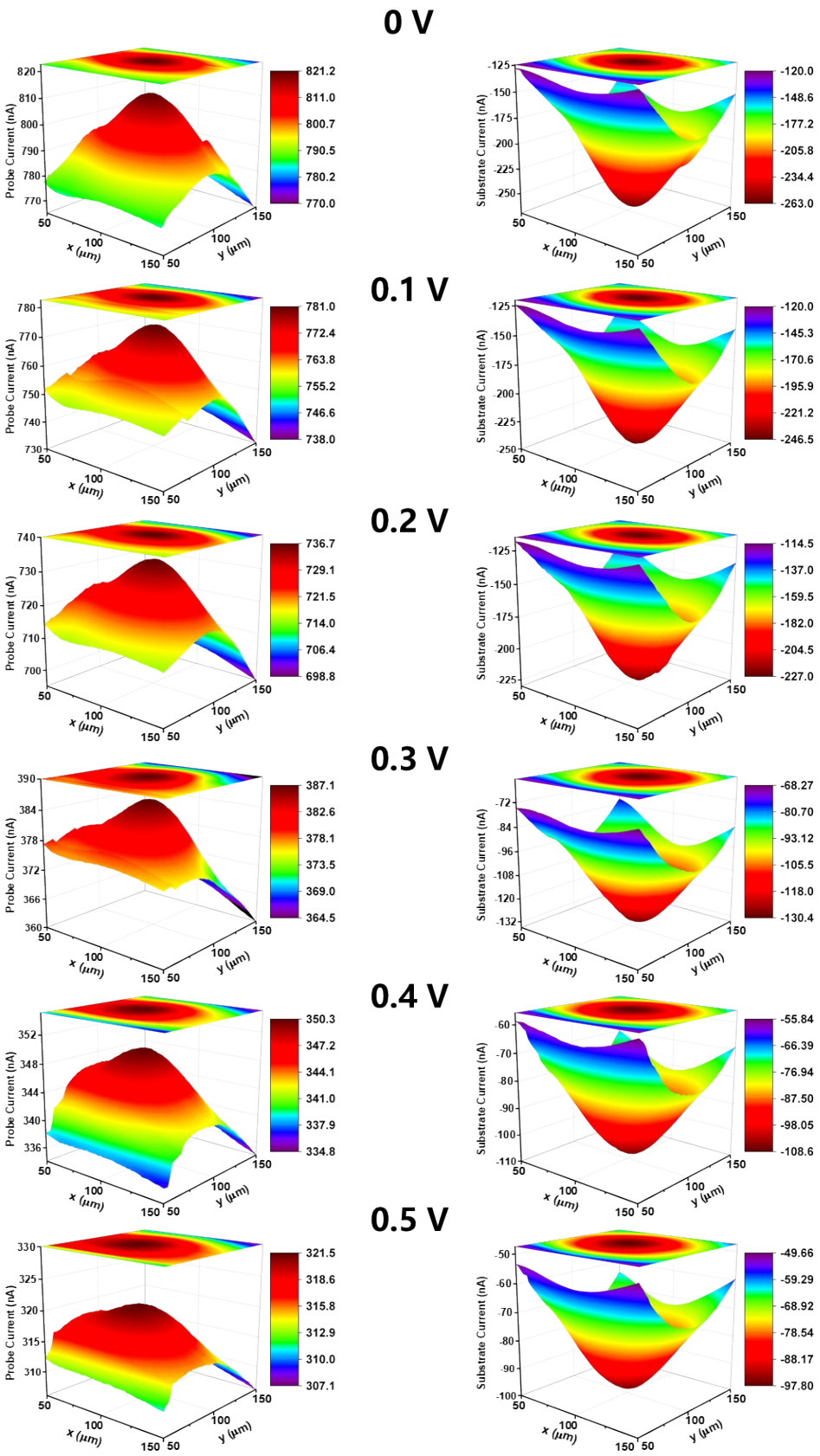

Figure S50. SECM images of CNT-Fe at substrate potential of 0.0 – 0.5 V (vs. RHE).

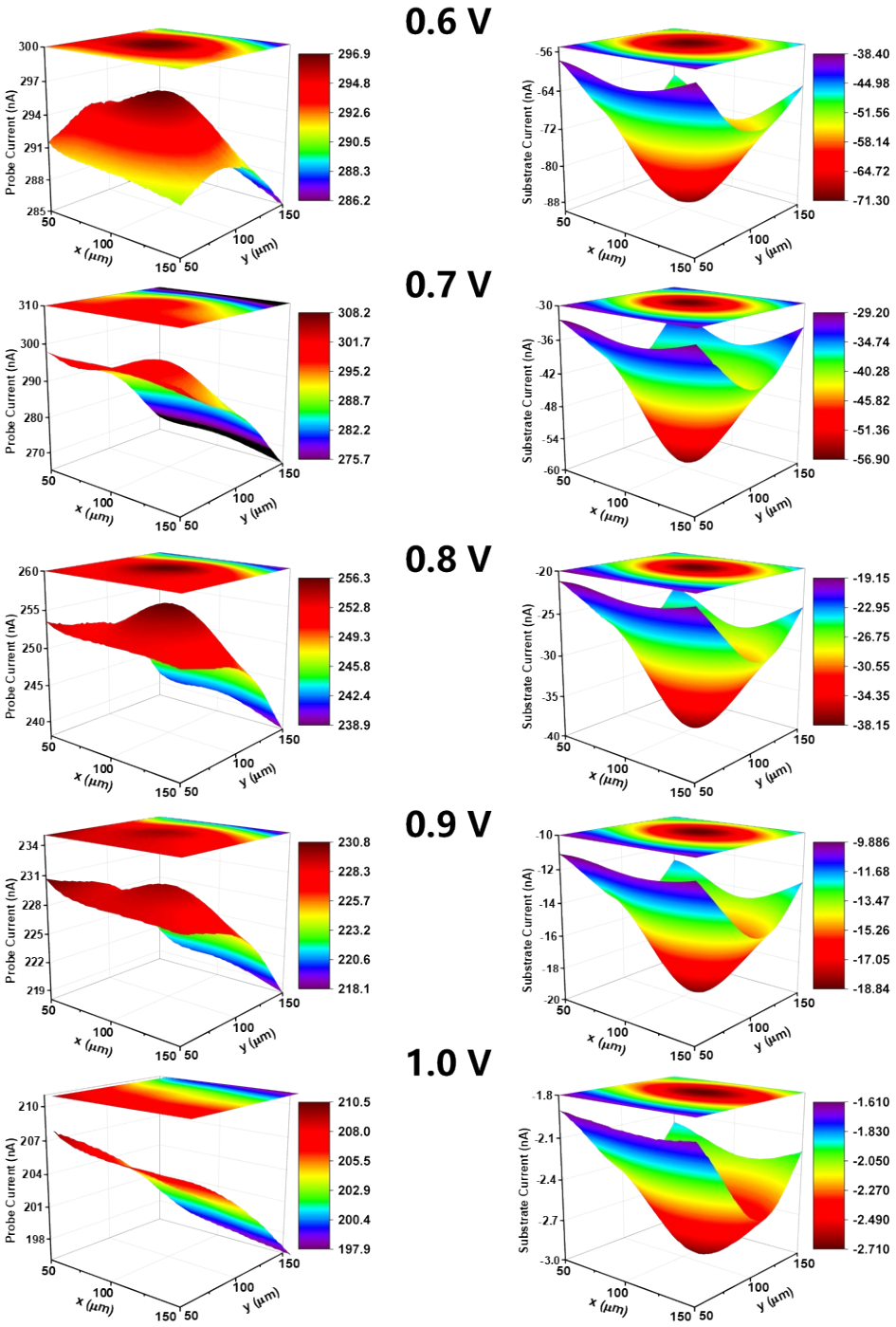

Figure S51. SECM images of CNT-Fe at substrate potential of 0.6 – 1.0 V (vs. RHE).

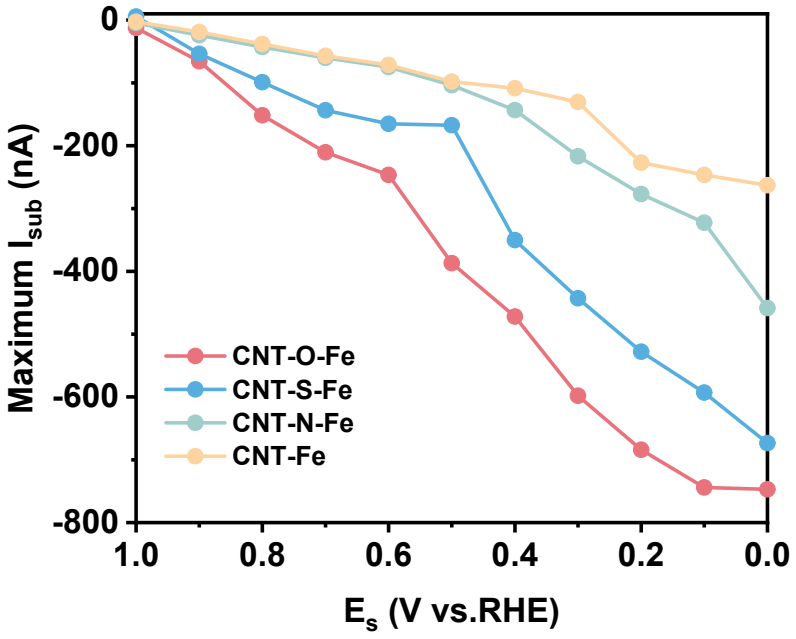

Figure S52. Plots of maximum substrate current as functions of substrate potential for SECM results.

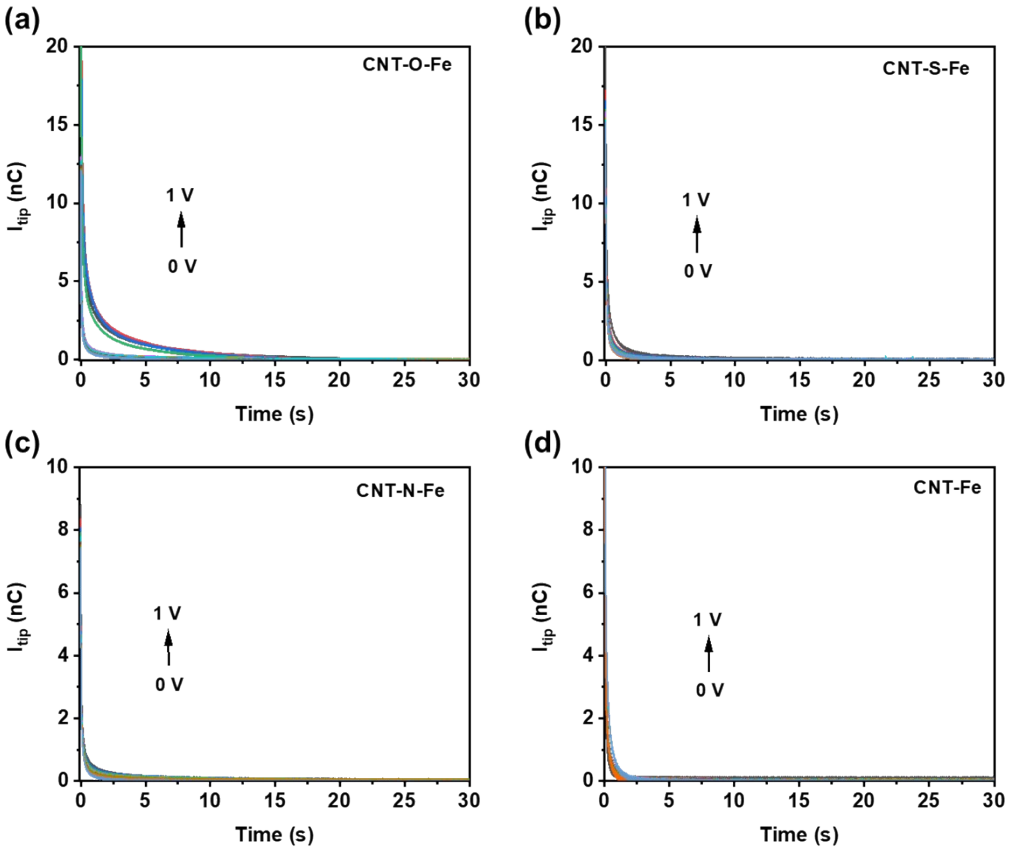

Figure S53. Chronoamperometry curves recorded on the tip in SI-SECM measurements of (a) CNT-O-Fe, (b) CNT-S-Fe, (c) CNT-N-Fe and (d) CNT-Fe.

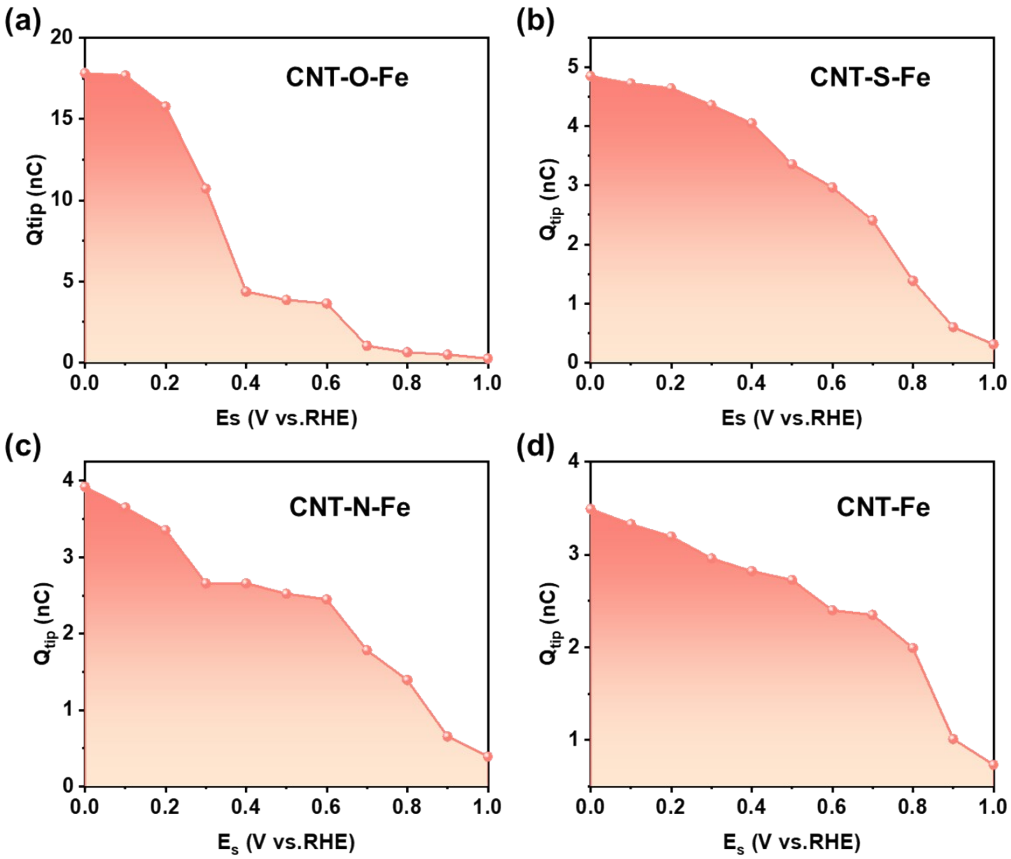

Figure S54. Integrated charge with SI-SECM of (a) CNT-O-Fe, (b) CNT-S-Fe, (c) CNT-N-Fe, and (d) CNT-Fe.

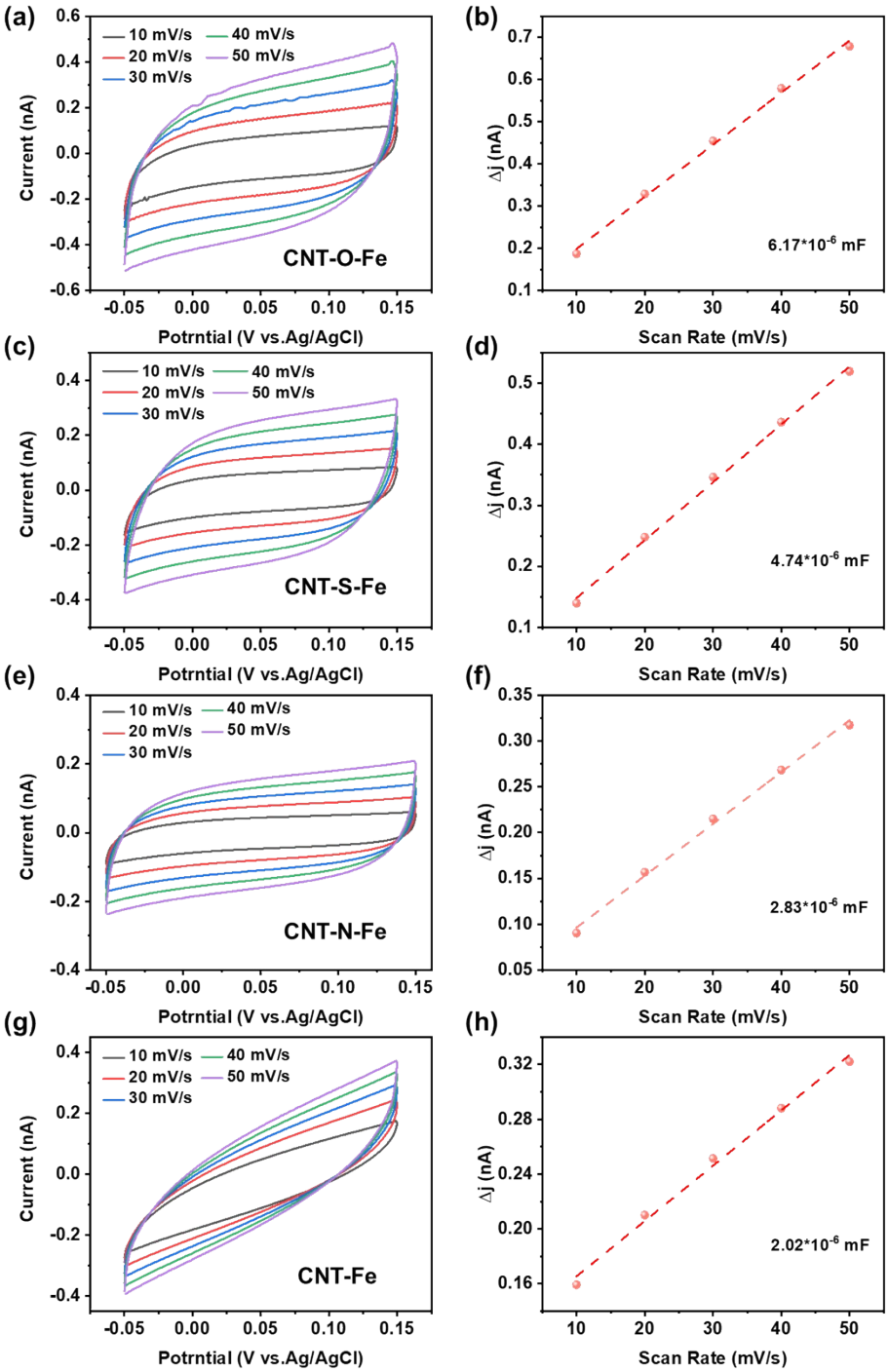

Figure S55. CV curves at different scan rates (left) and corresponding fitting results of C_{dl} (right) for (a-b) CNT-O-Fe, (c-d) CNT-S-Fe, (e-f) CNT-N-Fe, and (g-h) CNT-Fe on UME.

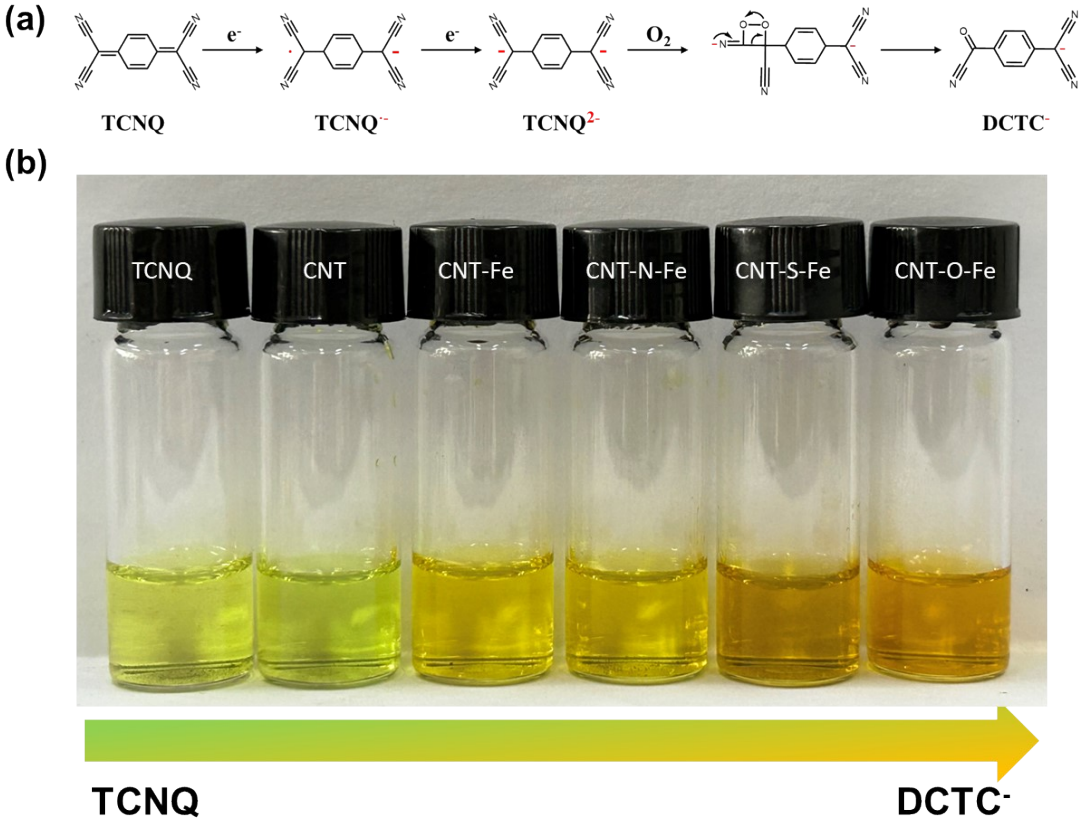

Figure S56. (a) Electron transfer reaction of TCNQ to $DCTC^-$. (b) Optical image of TCNQ solutions in acetonitrile and with CNT, CNT-Fe, CNT-N-Fe, CNT-S-Fe, and CNT-O-Fe.

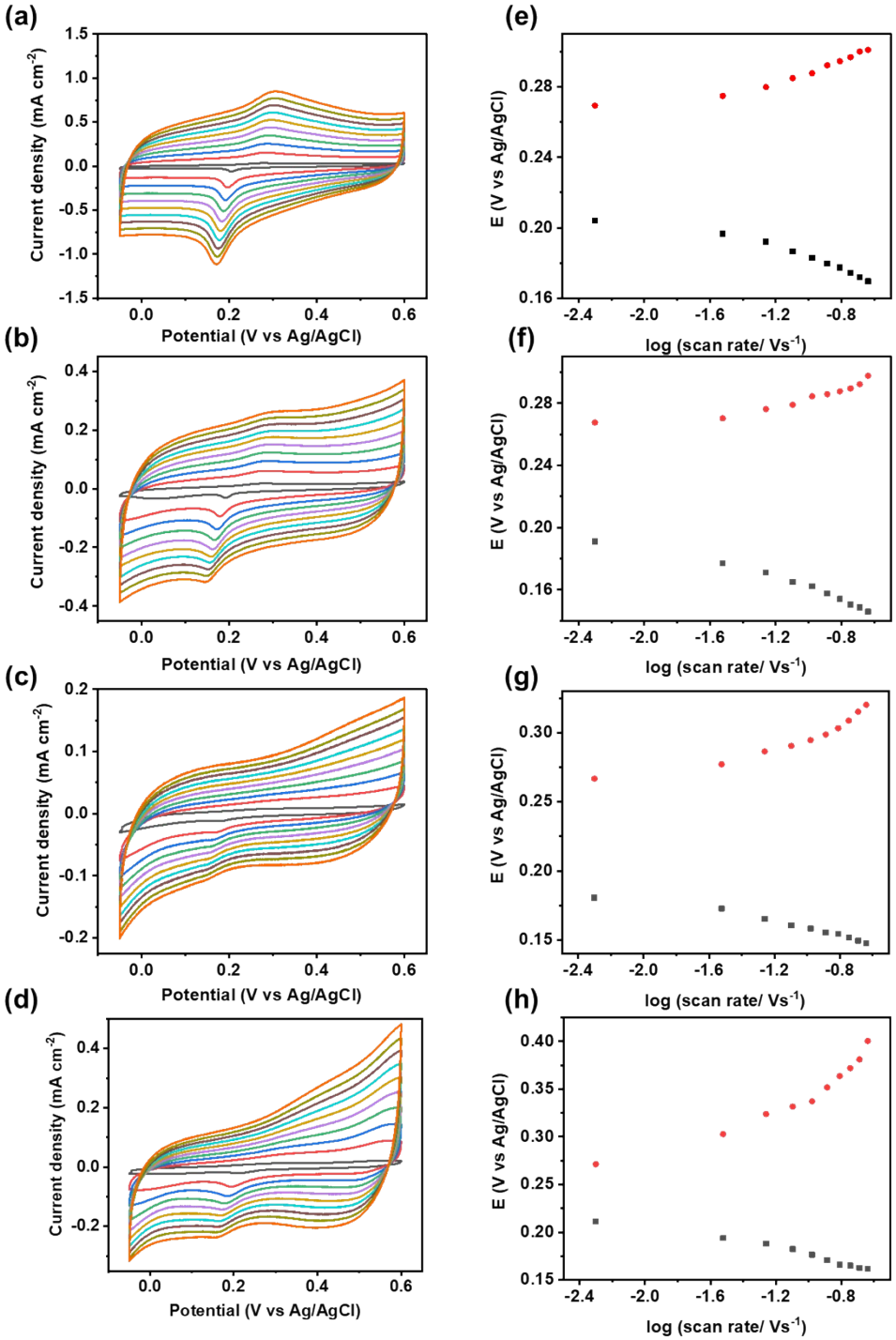

Figure S57. The $[Fe(CN)_6]^{3-}$ redox results of (a, e) CNT-O-Fe, (b, f) CNT-S-Fe, (c, g) CNT-N-Fe, and (d, h) CNT-Fe at different scanning rates (0.005-0.23 V/s) in 0.1 mol/L KCl tested on the glassy carbon electrode and the relationship between the position of redox peaks and the logarithm of scan rates.

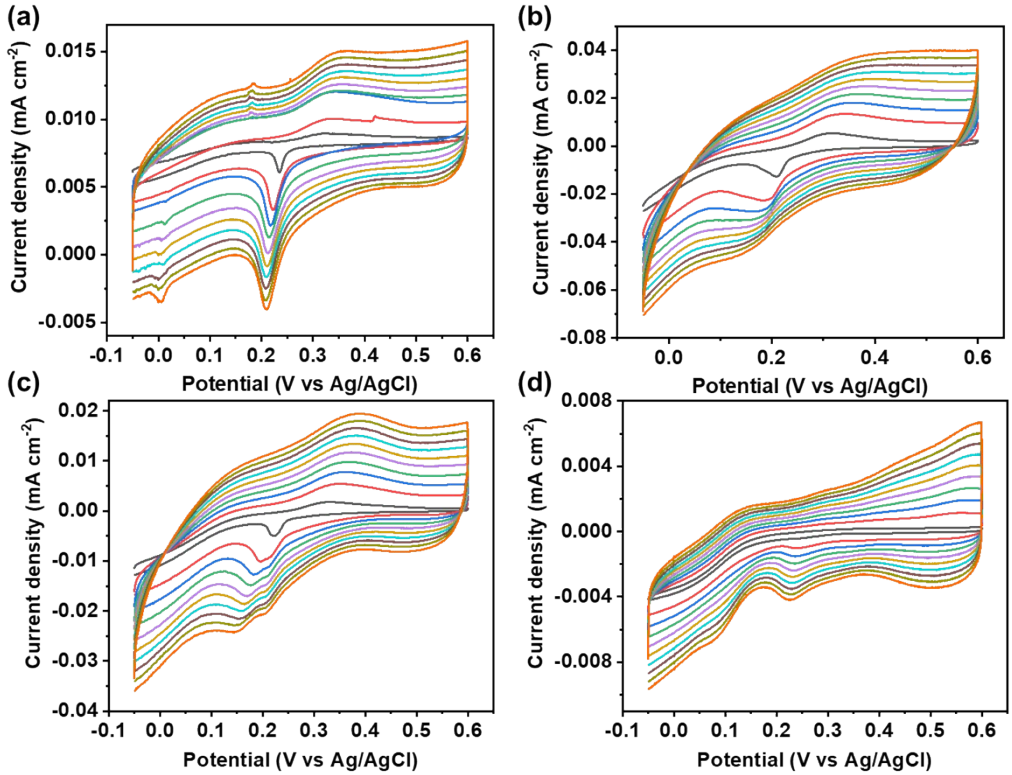

Figure S58. The $[Fe(CN)_6]^{3-}$ redox results of (a) CNT-O-Fe, (b) CNT-S-Fe, (c) CNT-N-Fe and (d) CNT-Fe at different scanning rates (0.005-0.23 V/s) in 0.1 mol/L KCl tested on the Au electrode

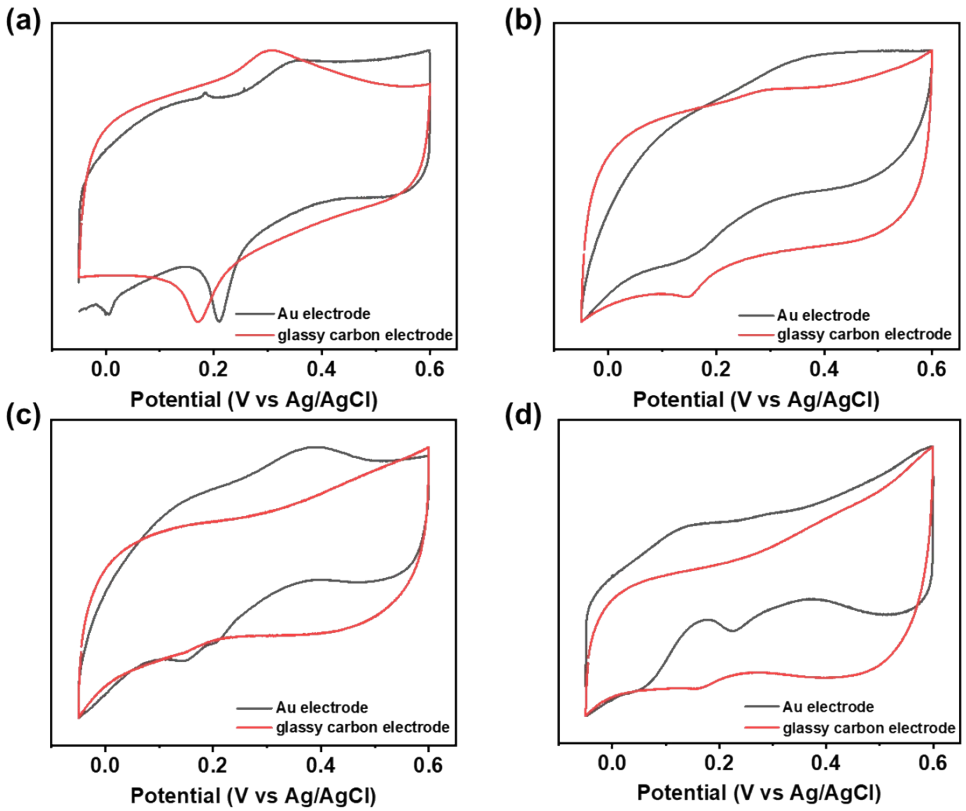

Figure S59. The comparison of $[Fe(CN)_6]^{3-}$ redox results of (a) CNT-O-Fe, (b) CNT-S-Fe, (c) CNT-N-Fe, and (d) CNT-Fe at different scanning rates (0.005-0.23 V/s) in 0.1 mol/L KCl tested on the Au electrode and glassy carbon electrode.

Table S1. Reaction free energy (eV vs. RHE) of elementary step for oxygen reduction at U_{RHE} = 0 V on different models.

	ΔG_1	ΔG_2	ΔG_3	ΔG_4	U^{RHE} onset
CNT-Fe	-0.17489	-1.72395	0.006698	0.04757	-0.04757
CNT-O-Fe	-0.10417	-1.04199	-0.5175	-0.18091	0.10417
CNT-S-Fe	-0.01202	-0.87676	-0.49738	-0.4584	0.01202
CNT-N-Fe	-0.43369	-1.14186	-0.28698	0.017957	-0.01796

Table S2. The net charges of Fe atoms in CNT-Fe and CNT-X-Fe obtained by Bader charge population analysis.

CNT-Fe	CNT-O-Fe	CNT-S-Fe	CNT-N-Fe
1.249 |e|	1.131 |e|	1.129 |e|	1.054 |e|

Table S3. Elemental compositions (C, N, O, Fe and S) obtained by XPS spectra.

	C (at%)	N (at%)	O (at%)	Fe (at%)	S (at%)
CNT-Fe	96.11	1.28	2.32	0.28	--
CNT-O-Fe	95.68	1.43	2.54	0.35	--
CNT-S-Fe	94.60	1.49	2.48	0.24	1.19
CNT-N-Fe	95.74	1.45	2.35	0.46	--

Table S4. EXAFS fitting parameters for CNT-X-Fe and CNT-Fe.

Samples	Bond type	Coordination number	R (Å)	σ^2 (10^{-3}Å^2)	R factor
CNT-Fe	Fe-N	4	1.98	7.4	0.03
CNT-O-Fe	Fe-N	4	1.96	1.0	0.01
	Fe-O	1	1.90	9.6	
CNT-S-Fe	Fe-N	4	1.95	8.5	0.01
	Fe-S	1	2.27	5.4	
CNT-N-Fe	Fe-N	4	1.96	5.8	0.02
	Fe-N	1	2.11	5.8	

Table S5. The $E_{1/2}$ for CNT-X-Fe catalysts with different mass ratios of $Fe(Phen)_2$ to CNT-X (1:4, 1:6, 1:8, 1:10).

Catalyst	1/4	1/6	1/8	1/10
CNT-O-Fe	0.78	0.85	0.84	0.82
CNT-S-Fe	0.78	0.82	0.79	0.76
CNT-N-Fe	0.76	0.81	0.80	0.73

Table S6. ORR performance of CNT-X-Fe and CNT-Fe.

Catalyst	E_{onset} (V)	$E_{1/2}$ (V)	Tafel slope (mV dec^{-1})	ECSA (m^2/g)
CNT-Fe	0.91	0.78	94.67	1.86
CNT-O-Fe	0.94	0.85	54.99	19.36
CNT-S-Fe	0.93	0.82	80.43	6.77
CNT-N-Fe	0.93	0.81	82.62	6.53

Table S7. Comparison of SD_{mass}, TOF and J_m for CNT-Fe and CNT-X-Fe.

Catalyst	TOF e $site^{-1}$ s^{-1})	SD_{mass} (10^{19} site g^{-1})	J_m (A g^{-1})
CNT-Fe	1.12	0.65	1.17
CNT-O-Fe	1.61	3.1	7.98
CNT-S-Fe	1.58	1.52	3.97
CNT-N-Fe	1.57	1.51	3.81

Table S8. The comparison of $[Fe(CN)_6]^{3-}$ redox results of CNT-Fe and CNT-X-Fe on the Au electrode and glassy carbon electrode.

	Glassy carbon electrode	Au electrode	
Catalyst	$\Delta E_{p\,(Gc)}$ (V)	$\Delta E_{p\,(Au)}$ (V)	$\lvert \Delta E_{p\,(Gc)} - \Delta E_{p\,(Au)} \rvert$
CNT-Fe	0.239	0.074	0.165
CNT-O-Fe	0.131	0.134	0.003
CNT-S-Fe	0.152	0.179	0.027
CNT-N-Fe	0.173	0.238	0.065

Reference

1. L. Li, X. Tang, S. Huang, C. Lu, D. Lützenkirchen-Hecht, K. Yuan, X. Zhuang and Y. Chen, *Angew. Chem. Int. Ed.*, 2023, **62**, e202301642.
2. X. Tang, Y. Wei, W. Zhai, Y. Wu, T. Hu, K. Yuan and Y. Chen, *Adv. Mater.*, 2023, **35**, 2208942.